Neodymium Isotope Constraints on the Origin of TTGs and High-K Granitoids in the Bundelkhand Craton, Central India : Implications for Archaean Crustal Evolution

Joshi, Kumar Batuk

2022-05-14

Joshi , K B , Singh , S K , Halla , J , Ahmad , T & Rai , V K 2022 , ' Neodymium Isotope Constraints on the Origin of TTGs and High-K Granitoids in the Bundelkhand Craton, Central India : Implications for Archaean Crustal Evolution ' , Lithosphere , vol. 2022 , no. Special 8 , 6956845 . https://doi.org/10.2113/2022/6956845

http://hdl.handle.net/10138/348423
https://doi.org/10.2113/2022/6956845

GeoScienceWorld
Lithosphere
Volume 2022, Article ID 6956845, 27 pages
https://doi.org/10.2113/2022/6956845

Lithosphere

Research Article

Neodymium Isotope Constraints on the Origin of TTGs and High-K Granitoids in the Bundelkhand Craton, Central India: Implications for Archaean Crustal Evolution

Kumar Batuk Joshi,[1,2] **Sunil Kumar Singh**,[2,3] **Jaana Halla**,[4] **Talat Ahmad**,[5] **and Vinai K. Rai**[2,6]

[1]*ESSO-National Centre for Earth Science Studies, Thiruvananthapuram, Kerala, India*
[2]*Geoscience Division, Physical Research Laboratory, Ahmedabad, India*
[3]*Director Office, National Institute of Oceanography, Goa, India*
[4]*Natural Sciences Unit, Finnish Museum of Natural History, University of Helsinki, Helsinki, Finland*
[5]*Vice Chancellor's Office, University of Srinagar, India*
[6]*School of Earth and Space Exploration, Arizona State University, USA*

Correspondence should be addressed to Kumar Batuk Joshi; kr.batukjoshi@ncess.gov.in

Received 22 September 2021; Accepted 12 April 2022; Published 14 May 2022

Academic Editor: Shuo Zhang

The Bundelkhand craton in central India consists mainly of abundant high-K granitoids formed at the Archaean-Proterozoic boundary and several enclosed rafts of TTGs (tonalite-trondhjemite-granodiorites) up to 3.5 Ga. Therefore, the Bundelkhand craton is a key locality for studies on Archaean crustal growth and the emergence of multisource granitoid batholiths that stabilised a supercontinent at 2.5 Ga. Based on their geochemical characteristics, the high-K granitoids are divided into low silica–high Mg (sanukitoids and hybrids) and high silica–low Mg (anatectic) groups. We aim to provide new insights into the role of juvenile versus crustal sources in the evolution of the TTG, sanukitoid, hybrid, and anatectic granitoids of the Bundelkhand craton by comparing their key geochemical signatures with new Nd isotope evidence on crustal contributions and residence times. The ages and geochemical signatures as well as εNd(t) values and Nd model ages of TTGs point towards partial melting of a juvenile or short-lived mafic crust at different depths. Paleoarchaean TTGs show short crustal residence times and contributions from the newly formed crust, whereas Neoarchaean TTGs have long crustal residence times and contributions from the Paleoarchaean crust. This may reflect the transition from melting in a primitive oceanic plateau (3.4-3.2 Ga) in plume settings, resulting in a Paleoarchaean protocontinent, to 2.7 Ga subduction and island arc accretion along the protocontinent. The 2.5 Ga high-K granitoids formed at convergent subduction settings by partial melting of the mantle wedge and preexisting crust. Sanukitoids and hybrid granitoids originated in the mantle, the latter showing stronger crustal contributions, whereas abundant anatectic granitoids were products of pure crustal melting. Our Nd data and geochemical signatures support a change from early mafic sources to strong crust-mantle interactions towards the A-P boundary, probably reflecting the onset of supercontinent cycles.

1. Introduction

The Earth's continents started to form four billion years ago in the Archaean Eon, and they grew larger through time. Over a very long time, ancient continents have joined, broken apart, and drifted around the globe multiple times into new configurations because of plate tectonics [1–3]. To understand the formation of the oldest continents, we need to study their fragments and correlate their chemical compositions and ages, which have been a great challenge and topic of debate for decades.

We know that, in the early Archaean, the main crust formation process was the episodic melting of basaltic crust that led to the formation of TTGs (tonalite-trondhjemite-

granodiorites) and building of the first continents [4]. The conditions under which the first continental crust formed were different from those presently operative. The mantle was hotter with smaller basaltic plates and faster convection rates [5]. Different conditions resulted in distinct geochemistry and isotope signatures of Archaean granitoids [6–11]. The geochemical composition of granitoids depends on various factors, including the physical and chemical conditions of the source, amount of residual minerals, varying anatectic conditions, stages of magmatic differentiation, and tectonic setting. Therefore, their compositional variation provides crucial information on the plate tectonic processes and crustal evolutionary history of the Early Earth [7, 10, 12–15]. The isotope systematics and geochemical signatures of granitoids provide insights into the age and nature of their source and role in crustal evolution.

Today, there is a general agreement that partial melting of hydrated basalts during the Archaean has produced the early felsic crust consisting mainly of silicic and sodic TTGs. However, the tectonic setting of TTGs is still controversial, and the views range from stagnant lid tectonics and plume tectonics involving mantle upwelling to arc tectonics related to subduction [16–20]. Some researchers favour partial melting of subducting oceanic slab and believe that the formation of Archaean protooceanic crust (hydrous metabasalt) and subsequent deep burial via subduction (a process similar to modern plate tectonics) can explain the generation of TTG melts at relatively great depths [17, 18, 21, 22]. Other researchers believe that TTGs could form in overthickened mafic crust [23] in island arc settings [24–26] or plume-related basalt plateaux [27–30]. Studies also suggest that the vertical growth of Archaean oceanic plateaux above mantle plumes can allow hydrothermal alteration of basalts required for TTG formation [31–34]. Recent studies suggest that TTGs can also be generated by fractional crystallization or by fractionation of melts derived from the enriched lithospheric mantle [35–37].

During the Meso- to Neoarchaean (3.0-2.5 Ga), the episodic melting in basaltic sources leading to the formation of TTGs declined, and a new type of multisource high-K calc-alkaline granitoids emerged as a consequence of changes in the Earth's geodynamics [14, 19]. These high-K granitoids are the second-most voluminous component of the Archaean crust after the TTGs. They are multisourced, ranging from the mantle or mixed mantle and crustal sources to pure crustal sources. They are formed by increasing crust-mantle interactions due to the onset of modern-type plate tectonics [8–10, 12, 38, 39]. Joshi et al. [9] divided high-K granitoids into two main groups, the Low Silica, High Mg (LSHM) group and the High Silica, Low Mg group (HSLM). The former includes mantle-derived sanukitoid granitoids and related hybrid granitoids formed by increased mantle-crust interactions, and the latter anatectic granitoids formed by pure crustal melting.

Geochemical signatures and geochronology of TTGs and high-K granitoids divide the Archaean crustal evolution into four main stages: (1) In the Eoarchaean, TTGs formed by episodic melting within the thin or thickened basaltic crust. 2) In the Paleoarchaean, TTG magmatism continued along with the formation of diorites and anatectic high-K granites, which caused the thickening of the crust. (3) In the Mesoarchaean, TTG formation continued and the first granitoids with mantle contributions, known as sanukitoids, appeared at around 3.0 Ga. (4) Neoarchaean was the time of granitoid diversification when TTG formation decreased and high-K magmatism increased indicating a significant geodynamic change that culminated in the Archaean-Proterozoic boundary [12]. In the Indian Shield, five cratons are the results of Paleoarchaean to Neoarchaean crustal growth (Figure 1). In this study, we focus on the Bundelkhand craton between the Aravalli and Bastar cratons in central India. This craton is a key research target because it includes Paleo- to Neoarchaean fragments of TTG crust embedded in abundant high-K granitoids formed at the Archaean-Proterozoic boundary. Therefore, the craton gives important knowledge on the evolution of the Paleoarchaean crust and the stabilisation of a supercontinent.

Recent studies have proposed a petrogenetic explanation of these diverse granitoid types based on whole-rock major and trace element geochemical and mineral chemistry [9, 40–42]. However, very few studies [43, 44] have focused on isotopic systematics to explain the plausible sources of the various granitoid varieties emplaced in the craton, and even fewer have compared the geochemical signatures with isotope results. In this contribution, we provide insights into the petrogenesis of the different types of the Bundelkhand granitoids by comparing new whole-rock Nd isotope results with compiled geochemical signatures and U-Pb ages. The aim is to correlate the geochemical fingerprints with the Nd isotope signatures to enlighten their source and tectonic setting. The Sm-Nd method has its limitations since the model ages are dependent on the suitability of the mantle model and the analytical uncertainties are relatively large. However, the $\varepsilon Nd(t)$ values and Nd-depleted mantle model ages have been successfully used in determining crustal formation ages, representing the approximate time when crustal blocks were first created by mantle-derived magmatism.

This study is aimed at providing significant information for defining the (1) Paleoarchaean and Neoarchaean evolution of the TTG crust, (2) stabilisation of the continental crust at the end of the Neoarchaean, and (3) the age, sources, and crustal contribution in the type formations of the Archaean-Proterozoic boundary. The last outcome can significantly contribute to the aims of the International Commission on Stratigraphy (ICS) in its efforts to define the border of the Archaean and Proterozoic Eons.

2. Regional Geology and Geochronology

There are five major Archaean cratons in two distinct crustal blocks in the Indian Shield (Figure 1), the Northern and Southern Blocks separated by the Central Indian Tectonic Zone (CITZ). The former consists of the Bundelkhand and Aravalli cratons, while the latter consists of the Dharwar, Singhbhum, and Bastar cratons. Figure 1 shows a generalized geological map of the Bundelkhand craton with an inset showing the different cratons of the Indian Shield. The semicircular body of the Bundelkhand craton is bounded by the

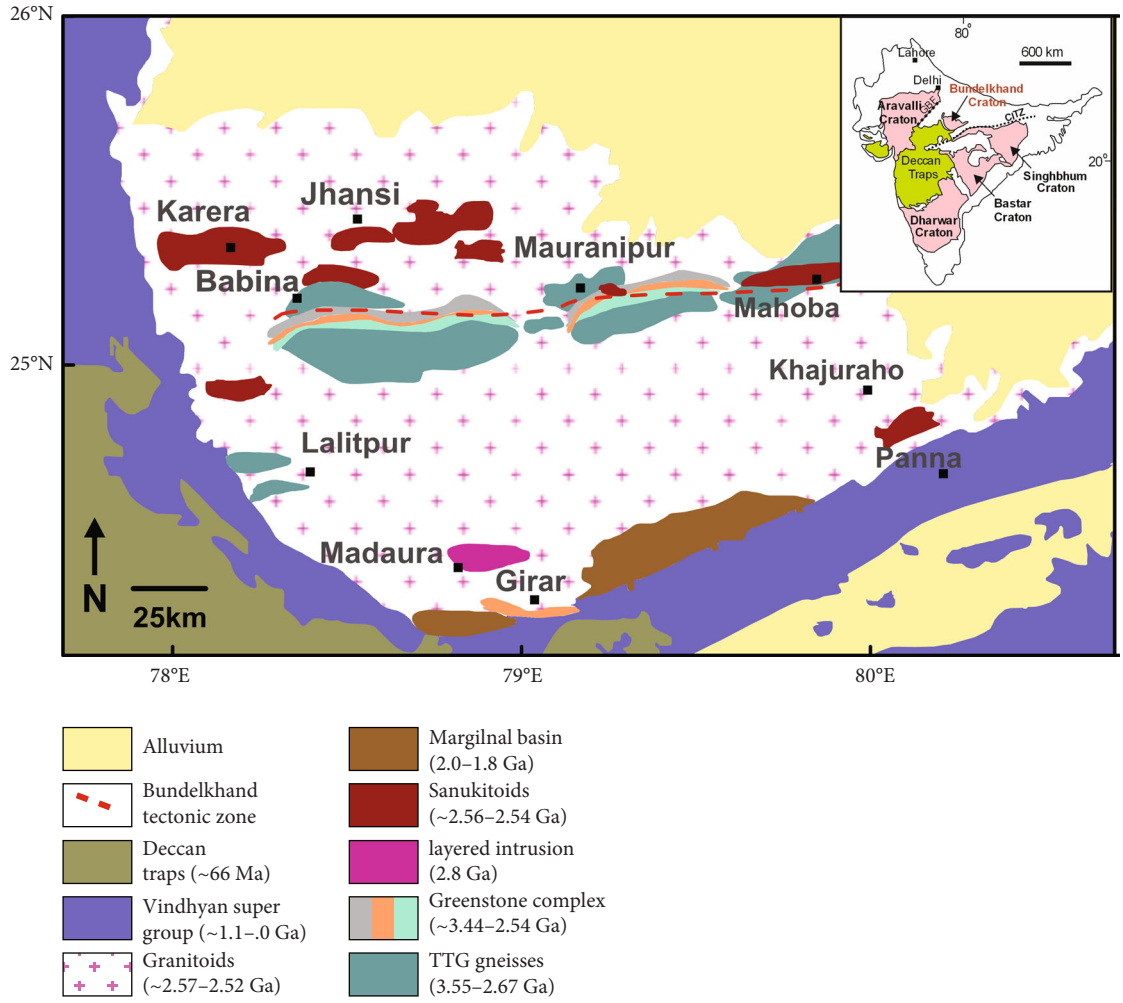

Figure 1: Generalized geological map of the Bundelkhand craton after [9, 45, 51]. The inset shows an outline map of India showing the different cratons of the Indian Shield, modified after [47, 100].

Paleoproterozoic (2.0–1.8 Ga), Gwalior (Northwest), Sonrai (South) and Bijawar (Southeast) basins which are overlain by the Mesoproterozoic Vindhyan Supergroup that occurs on three sides of the craton. The northern side of the Bundelkhand craton is covered by Indo-Gangetic alluvial plains [45–47].

The dominant lithology in the Bundelkhand craton (Figure 1) consists of Neoarchaean potassic granites, which are intruded into Paleo-Mesoarchaean TTG gneisses and supracrustal units. The E-W-trending Bundelkhand tectonic zone (Figure 1) divides the craton into three segments, viz., (i) the central Bundelkhand granite-greenstone terrane, (ii) the southern Bundelkhand granite-greenstone terrane, and (iii) the north Bundelkhand granitoid terrane [48–51]. The central Bundelkhand granite-greenstone terrane extends from Mahoba to Babina and consists of TTGs, volcano-sedimentary sequences, and high-K granitoids (including sanukitoids) [9, 40, 43, 44, 52–59]. The southern Bundelkhand granite-greenstone terrane consists of quartzite, BIF, chlorite schist, and marble and extends from Rungaon to Girar [48, 51, 60–62]. Mafic dyke swarms and giant quartz veins traverse the above lithologies and represent the last magma-related hydrothermal activity in the Bundelkhand craton [52, 63–66].

Table 1 presents compiled geochronological data from the Bundelkhand craton [9, 43, 44, 48, 52, 54–58, 67–70]. The oldest rocks in the Bundelkhand craton are Paleo- to Neoarchaean TTGs showing distinct formation episodes at ca. 3.56 Ga, 3.44 Ga, 3.3 Ga, 3.2 Ga, and 2.71-2.68 Ga. Singh and Slabunov [48] and Slabunov and Singh [62] dated felsic volcanics from Babina and Mauranipur at 2.54, 2.56, and 2.81 Ga, respectively, while the mafic-ultramafic rocks from Babina have yielded a Sm-Nd isochron age of 3.4 Ga [50]. The TTGs occur as east-west-trending rafts within abundant high-K granitoids, the dominant rock type of the craton emplaced at the 2.5 Ga Archaean-Proterozoic boundary.

3. Bundelkhand Granitoids

3.1. Geochemical Signatures and Classification. The granitoids of the Bundelkhand craton show typical geochemical characteristics of TTGs, sanukitoids, and anatectic

Table 1: Compiled geochronological data from the Bundelkhand craton.

Rock type	Area	Age (Ma)	U-Pb method	Reference
Gneiss	Mahoba	3041 ± 8 Ma; 3270 ± 3 Ma	Ion probe $^{207}Pb/^{206}Pb$	Mondal et al. [56]
	Kuraicha	3297 ± 8 Ma; 2884 ± 15 Ma		
	Babina	2697 ± 3 Ma		
	Panchwara	3189 ± 5 Ma	Ion probe $^{207}Pb/^{206}Pb$	Mondal et al. [101]
	Karera	2563 ± 6 Ma		Mondal et al. [56]
	Baghora	3503 ± 99 Ma	Rb-Sr whole rock	Sarkar et al. [69]
	Dinara, Bedaura, Panchaura	2561 ± 11 Ma; 2551 ± 7 Ma; 2546 ± 6 Ma	LA-ICPMS	Kaur et al. [55]
TTG	Sukwa Dukwa dam	3397 ± 8 Ma; 3390 ± 16 Ma	SHRIMP U-Pb	Nasipuri et al. [57]
TTG	Kuraicha, Roni, Rungaon, Mahoba	3551 ± 6 Ma; 3394 ± 9 Ma; 3205 ± 12 Ma; 3285 ± 7 Ma	LA-ICPMS	Kaur et al. ([54], [55])
TTG	Babina	3589 ± 8 Ma; 3440 ± 3 Ma	LA-SF-ICPMS	Saha et al. [58]
TTG	Babina	2669 ± 7 Ma	LA-SF-ICPMS	Verma et al. [70]
TTG	Mauranipur	3414 ± 17 Ma	LA-ICPMS	Colleps et al. [52]
TTG	Near Mahoba	3301 ± 2 Ma; 3327 ± 5 Ma	SIMS U-Pb	Joshi et al. [9]
TTG	Baragaon	3411 ± 9 Ma	LA-ICPMS	Singh et al. [43]
TTG	Roni	3343 ± 85 Ma; 3422 ± 39 Ma; 3364 ± 10 Ma		
TTG	Charkhari, Mahoba	3280 ± 15 *Ma*; 3366 ± 10 *Ma*		
TTG	Babina	2681 ± 10 *Ma*; 2706 ± 11 *Ma*		
TTG	Kuraicha	2712 ± 16 Ma		
TTG	Central Bundelkhand	3291 ± 5 Ma	SHRIMP U-Pb	Kumar et al. [102]
TTG migmatite	Mauranipur	Rim: 2700 ± 16 Ma; core: 3478 ± 48 Ma	SHRIMP U-Pb	Kumar et al. [41]
TTG migmatite	Babina	2685 ± 8 Ma	SHRIMP U-Pb	Kumar et al. [102]
Closepet type granodiorite (sanukitoid)	Orchha	2553.3 ± 13 Ma; 2925 ± 25 Ma (inheritance)	SIMS U-Pb	Joshi et al. [9]
Sanukitoid type monzogranite (sanukitoid)	Khajuraho	2537.4 ± 11 Ma		
High Mg granitoid (sanukitoid)	Near Jhansi	2563.6 ± 2 Ma		
		2559.4 ± 7.3 Ma		
Low-HREE monzogranites	Near Jhansi	2562 ± 25 Ma; 2797 ± 9 Ma (inheritance)		
		2552 ± 30 Ma		
Low-Eu monzogranites	Mauranipur			

Table 1: Continued.

Rock type	Area	Age (Ma)	U-Pb method	Reference
		2571 ± 28 Ma; 3588 ± 27 Ma (inheritance)		
	Near Talbehat	2544 ± 3 Ma		
	Babina	2547 ± 3 Ma		
Monzogranite	Near Khajuraho	2565 ± 11 Ma		
	Bijoli	2555 ± 9 Ma		
Sanukitoid	Jhansi	2568 ± 12 Ma		
Anatectic granite	Babina	2556 ± 23 Ma	LA-ICPMS	Singh et al. [43]
	Bbaghora, Babina	2557 ± 16 Ma		
Leucogranitoids	Lalitpur	2492 ± 10 Ma		
Hornblende granite	Lalitpur	2521 ± 7 Ma		
	Datia	2515 ± 5 Ma	Ion probe $^{207}Pb/^{206}Pb$	Mondal et al. [56]
Leucogranitoids	Jakhaura	2516 ± 4 Ma		
	Mahoba	2454 Ma to 2551 Ma		
Syenogranite		2526 ± 7 Ma		
Monzodiorite		2536 ± 4 Ma	SHRIMP U-Pb	Kumar et al. [102]
Granodiorite		2545 ± 5 Ma		
Granite	Kalothra, Jhansi, Lalitpur, Kuraicha, Dinara	2583 ± 10 Ma; 2529 ± 8 Ma; 2566 ± 14 Ma; 2564 ± 42 Ma; 2545 ± 10 Ma; 2523 ± 10 Ma		
Granite	Patha Bharthari, Vijaipur, Baghora, Mauranipur	2543 ± 10 Ma; 2537 ± 8 Ma; 2525 ± 25 Ma; 2548 ± 8 Ma	LA-ICPMS	Kaur et al. [55]
Granite	Charkhari-Kabrai, Chattarpur-Tikamgarh	2549 ± 13 Ma; 2516 ± 35 Ma		
Granite	Chayyan, Panchaura, Utwaha	2591 ± 17 Ma; 2539 ± 7 Ma; 2554 ± 5 Ma		
Granite	Babina	2531 ± 21 Ma; 2516 ± 38 Ma; 2514 ± 13 Ma	LA-ICPMS	Verma et al. [70]
Granite	Jhansi-Panna	2545 ± 75	ID-TIMS-Rb-Sr whole rock	Crawford [67]
Granite	Mahoba	2540 ± 7 Ma	SHRIMP	Kumar et al. [41]
Granitoid	Chitrakoot hillock	2583 ± 1 Ma		
Granitoid	Panna	Between 2482 ± 11 Ma and 2603 ± 12 Ma	LA-ICPMS	Colleps et al. [52]

Table 1: Continued.

Rock type	Area	Age (Ma)	U-Pb method	Reference
Granitoid	North of Bijawar	2525 ± 18 Ma		
Granitoid	Mahoba	2544 ± 4 Ma		
Granitoid	Near Jhansi	2550 ± 6 Ma		
Rhyolite	Bansi	2521 ± 7 Ma	Ion probe $^{207}Pb/^{206}Pb$	Mondal et al. [101]
Granodiorite	Sakrar	2577 ± 16 Ma	LA-ICPMS	Singh et al. [50]
Felsic volcanics	Mauranipur	2810 ± 13 Ma; 2557 ± 33 Ma	SHRIMP	Slabunov and Singh [62]
Felsic volcanics	Near Babina	2542 ± 17 Ma	SHRIMP	Singh and Slabunov [48]
Ultramafic	Babina	3435 ± 16 Ma	ID-TIMS Sm-Nd whole rock	Singh et al. [50]
Metasomatic rocks	Mauranipur	2687 ± 11 Ma	SHRIMP	Slabunov and Singh [62]
Mafic dyke	—	1979 ± 8 Ma	LA-ICPMS	Pradhan et al. [103]
Dolerite dyke	Chitrakoot hillock	2551 ± 1 Ma		
Mafic intrusive	Near Jhansi	2556 ± 2 Ma	LA-ICPMS	Colleps et al. [52]
Mafic intrusive	Near Jhansi	2561 ± 1 Ma		

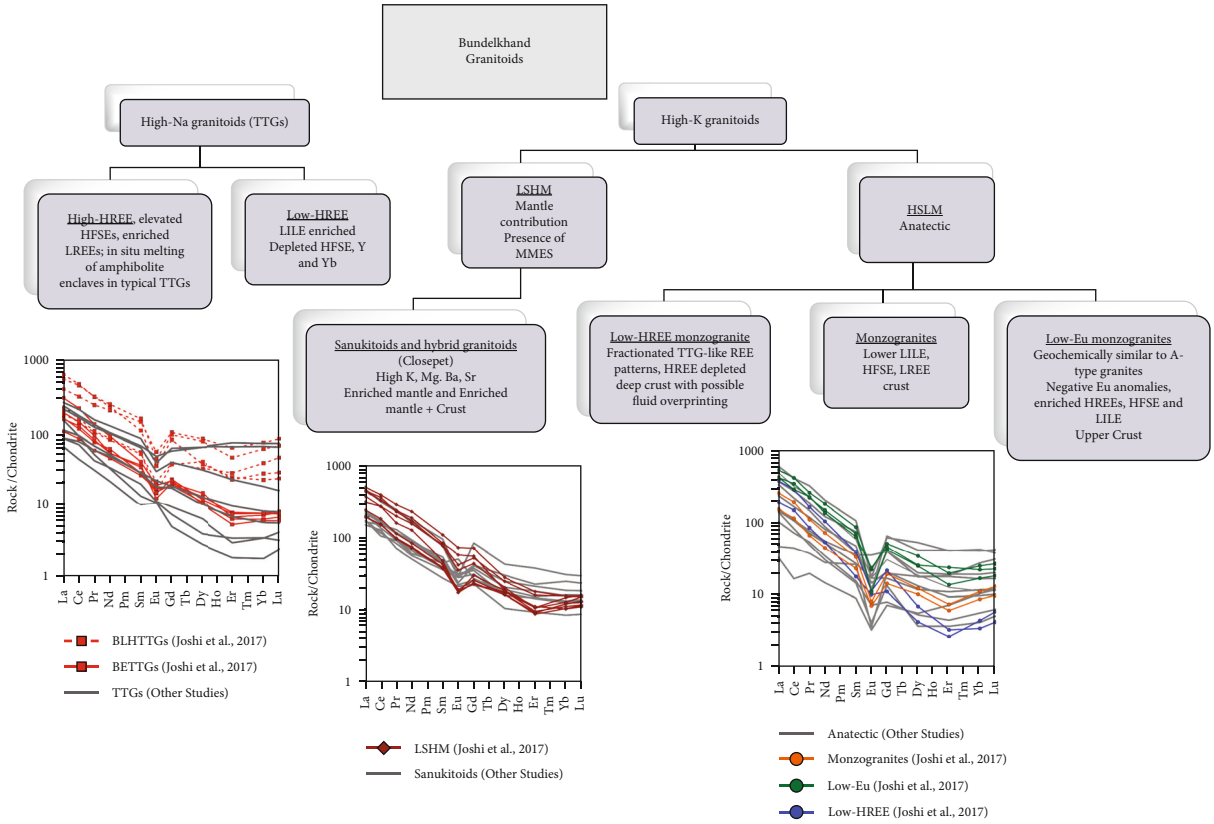

Figure 2: A classification scheme for the Bundelkhand TTGs and high-K granitoids ([9]).

granitoids. Full geochemical datasets, ages, and explanations for the Bundelkhand granitoid samples that are analysed for Nd in this study are available in the works of Joshi et al. [9, 40]. In this paper, we address the possible source characteristics of the Bundelkhand granitoids in terms of the geochemical signatures or fingerprints suggested for Archaean granitoids based on data compiled from several cratons [12].

(1) *Mantle signature* (low SiO_2 contents and high contents of mantle-compatible elements Mg, Cr, and Ni) can be observed in mantle-derived granitoids

(2) *Basaltic crust signature* (high Na, high SiO_2 contents, and low contents of mantle-compatible elements) in granitoids derived from basaltic precursors

(3) *Enriched mantle signature* (high Mg-K-Ba-Sr-P and LREE), inherited from Archaean mantle overprinted by crust-mantle interactions, is typical for sanukitoid granitoids. This signature cannot be a consequence of fractional crystallization, because it is independent of the SiO_2 content and can be also found in mafic rocks, such as lamprophyres, which are often associated with sanukitoids

(4) *Garnet fingerprint* (low Y and HREE, high Gd/Er) derived from garnet-bearing sources, where garnet is retained in the residue (e.g., deep lower crust). Thus, the presence or absence of this fingerprint reflects the depth of melting

(5) *Continental crust signature* (high SiO_2 and K_2O contents, mantle and enriched mantle signatures absent) in continental crust-derived granitoids

The geochemical classification scheme of Joshi et al. [9] in Figure 2 divides the Bundelkhand granitoids into two main groups: high-Na TTGs (~3.5-2.6 Ga) and high-K granitoids (~2.5 Ga). The TTG group carries the basaltic crust signature and consists of low-HREE and high-HREE end members (garnet fingerprint present or absent, respectively). The key geochemical signatures of the low-HREE group are LILE enrichment and depletion in HFSE, Y, and Yb, whereas the high-HREE group shows elevated HFSEs and enrichment in LREE. The silica and magnesium contents of the high-K granitoids further divide them into LSHM (Low Silica, High Mg) and HSLM groups. The LSHM group shows enriched mantle signatures and mafic magmatic enclaves. The strength of the mantle signature may vary from high in sanukitoid granitoids to lower in hybrid ("Closepet-type") granitoids formed by stronger crust-mantle interactions. The HSLM group consists of anatectic granitoids with a continental crust signature. Specific geochemical characteristics divide this group into low-HREE monzogranites from deep HREE-depleted crust, monzogranites (biotite granites) from the middle crust, and A-type granites with strong negative Eu anomalies from the upper crust.

3.2. Sample Descriptions. The detailed field descriptions, major and trace element geochemistry, and U-Pb zircon geochronology of TTGs and high-K granitoids analysed for Nd isotope compositions in this study can be found in the work by Joshi et al. [9, 40]. A summary of the sample locations and descriptions of the studied granitoid varieties is given in Table 2 while field and petrographic images are shown in Figures 3 and 4. The TTGs are exposed as E-W-trending slivers in Mahoba, Mauranipur, and Babina. They are deformed coarse-grained heterogeneous bodies, typically exhibiting alternating layers of leucocratic and melanocratic bands (Figure 3(a)) and are occasionally homogeneous (Figure 3(b)). The TTGs are inequigranular and consist of coarse-grained plagioclase (45 vol%), quartz (22 vol%), K-feldspar (18 vol%), biotite (10 vol%), and amphibole (5 vol%) (Figures 4(a) and 4(b)) with minor amounts (1 vol%) of titanite, epidote, apatite, and zircon.

The high-K group consists of grey or pink, fine- to coarse-grained, and occasionally porphyritic granitoids (Figures 3(c)–3(f)). Sometimes, the high-K granitoids are slightly deformed and show an alignment of mafic minerals. In the LSHM varieties, the K-feldspar dominate over plagioclase. Mineral abundances depict a higher quartz content (27 vol%) as compared to TTGs, plagioclase (35 vol%), K-feldspar (15 vol%), and the presence of amphibole (15 vol%) and biotite (7 vol%) as major minerals (Figures 4(c)–4(f)). The common accessory minerals (1 vol%) in LSHM varieties include zircon, titanite, epidote, and apatite. The HSLM varieties have a very similar mineral composition [K-feldspar (35 vol%), quartz (40 vol%), plagioclase (22 vol%), and biotite (2 vol%)] with accessory phases like amphibole, titanite, epidote, apatite, and zircon (1 vol%), but they have low to negligible amphibole content and, occasionally, fine-grained groundmass with phenocrysts of quartz and feldspar (Figure 4(f)).

4. Analytical Techniques

Approximately 200 mg of whole-rock powder was first decomposed in a mixture of HF-HNO_3-HCl in microwave digestion. The solution was further transferred in Savillex® vials and digested repeatedly with HF-HNO_3-HCl at ~100°C to bring the powder to complete solution. The acid digestion step was repeated as needed to ensure the complete digestion of the sample. Post digestion, the solution was dried and divided into two aliquots by weight. A known amount of ^{149}Sm and ^{145}Nd spikes by isotope dilution was added to the first aliquot, and Sm and Nd concentrations were measured by QICP-MS (Thermo Xseries-2) at the Physical Research Laboratory (PRL), Ahmedabad, India. The second aliquot was used to separate Nd by cation exchange columns, following standard ion-exchange procedures [71], ^{143}Nd/^{144}Nd ratios were measured on a Finnigan Neptune MC-ICP-MS at PRL, and the analyses were carried out in static multicollection mode. Mass fractionation corrections were made by normalising ^{143}Nd/^{144}Nd ratios to ^{146}Nd/^{144}Nd = 0.7219. The JMC for the Nd (^{143}Nd/^{144}Nd) isotope standard was measured during analyses which yielded values of 0.710343 ± 0.000002 (1σ, $n = 7$; σ = standard deviation) and 0.511714 ± 0.000004 (1σ, $n = 15$). Total procedural blanks for Nd were several orders of magnitude lower than typical total Nd loads analysed, and hence, no corrections for blanks were made.

The single-stage Nd model age (T_{DM1}), also known as "crustal extraction/formation age" or "crustal residence age," is the time elapsed since the Nd in the rock separated from the mantle. In the case of single-stage Nd model ages, it is assumed that crustal processes like metamorphism and intracrustal melting have not changed the Sm/Nd ratios. Archaean granitoids might have suffered multiple melting episodes of magma mixing, melting, fractional crystallization, and alteration. Therefore, to correct for changes in Sm/Nd ratios produced by crustal processes, two-stage depleted mantle Nd model ages (T_{DM2}) were calculated using the present-day depleted mantle ^{143}Nd/^{144}Nd and ^{147}Sm/^{144}Nd values of 0.51315 and 0.2136 and decay constant value of 6.54×10^{-12} a^{-1}, and the rock formation ages [72] suggested that the two-stage model ages give more consistent ages. The depleted mantle (DM) has been calculated using the linear depletion model, which assumes linear depletion from εNd = 0 at ~4.56 Ga to +10 today. The isotope compositions of samples from Bundelkhand granitoids are presented in Table 2.

5. Results

The Sm-Nd results on 44 whole-rock samples of TTGs and high-K granitoids are shown in Table 3. We calculated εNd(t) values based on U-Pb zircon data from Joshi et al. [9] and unpublished ages, on the same sample or samples within the same geochemical group. Fifteen samples of Paleoarchaean TTGs (3.4-3.3 Ga) show positive εNd (3345 or 3335) values from 0.54 to 1.96 and the Nd two-stage depleted mantle (T_{DM2}) model ages from 3592 to 3397 Ma. Neoarchaean TTGs, on the other hand, show mostly negative εNd (2713) values ranging from 0.36 to -2.61 and Nd (T_{DM2}) model ages of 3314-2965 Ma. The 2.57-2.53 Ga high-K LSHM granitoid group (15 samples of sanukitoids and hybrids) shows εNd(t) values from -3.60 to 3.13 (Table 3). Their Nd (T_{DM2}) model ages vary within a relatively smaller range from 3144 to 2619 Ma. The 2.59-2.54 Ga high-K HSLM varieties (18 samples) show εNd(t) values ranging between -0.30 and -5.89 and Nd (T_{DM2}) model ages ranging from 3190 to 2820 Ma.

The εNd(t) values and zircon ages for the TTG, LSHM, and HSLM granitoids of this study together with compiled data from Bundelkhand, Dharwar, and Aravalli cratons are shown in Figure 5. The positive εNd(t) values indicate derivation from a juvenile source or a short-lived mafic crust, while the negative εNd(t) values point towards crustal inputs. A large gap between the model and crystallization ages point to large crustal residence times and a dominant role of the older continental crust.

6. Discussion

The granitoids of the Bundelkhand craton show a wide range in composition and ages from Paleoarchaean high-Na TTGs to abundant high-K granites emplaced at the

Table 2: Field descriptions and petrography of the Bundelkhand granitoids.

Sample no.	Location	Description	Mineralogy
TTGs			
BLHTTG 4*/BTTG 123	Jaunpur near Babina	Migmatised TTGs with alternate quartzofeldspathic and mafic bands	Pl (~44 vol%), Qtz (~22 vol %), Kfs (~18 vol%), Bt (~10 vol %), and Hbl (~5 vol %); accessory minerals: titanite, epidote, apatite, and zircon (~1 vol%)
BLHTTG 2	Near Sukwa Dukwa	Migmatised gneiss intruded by porphyritic granites (HSLM granitoids)	
BLHTTG 3	Near Sukwa Dukwa	Migmatised gneiss intruded by porphyritic granites (HSLM granitoids)	
BLHTTG 1	Jaunpur near Babina	Migmatised TTGs with alternate quartzofeldspathic and mafic bands	
BLHTTG 7	Near Sukwa Dukwa	Migmatised gneiss intruded by porphyritic granites (HSLM granitoids)	
BETTG 1	Kua Gaon	Slightly migmatised TTGs with alternate quartzofeldspathic and mafic bands	
BETTG 107*	Karara, near Mahoba	Migmatised TTGs intruded by sanukitoid granodiorites (LSHM); these are occasionally cut by pegmatite veins	
BETTG 11*/BETTG 133	Mauranipur	Slight to moderately migmatised TTGs; localised melting is evident by the presence of leusosomes and malenosomes at places the TTGs are relatively homogeneous	
BETTG 3	Karara, near Mahoba	Migmatised TTGs intruded by sanukitoid granodiorites (LSHM); these are occasionally cut by pegmatite veins	
BETTG 5	Karara, near Mahoba		
BETTG 9	Karara, near Mahoba		
BC.16	Baragaon	TTG exposures are coarse grained and heterogeneous comprising of alternating quartzofeldspathic and mafic bands (typical gneissic banding)	Pl (58–60%), Qtz (31–33%), Hbl (2–3%), Bt (2–3%), Kfs; some samples have abundant biotite
BC.45	Roni village	Strongly deformed, light grey, coarse-grained gneissic TTG with alternate light and dark bands at places	
BC.60	Charkhari, Mahoba	The rock exposure shows gneissic layering which consists of alternate quartzofeldspathic and mafic bands that are folded	
BC.61	Raksa	Heterogeneous bodies consisting biotite rich and quartzofeldspathic bands	
BC.27	Babina	Sporadic exposures of TTG gneiss are weakly foliated light grey to whitish in color and show compositional banding	
Low silica high magnesium granitoids/sanukitoids and hybrids			
BCTG 129*	Orchha	Light grey deformed granitoids with occasional presence of schlieren; occasionally intruded by pegmatites	Kfs (~15 vol%), Qtz (~27 vol%), Pl (~35 vol%), Hbl (~15 vol%), and Bt (~7 vol%) with accessory phases like titanite, epidote, apatite, and zircon (~1 vol%)
BCTG 101	Orchha (near station)	Grey colored, slightly deformed coarse-grained granite	
BCTG 27	Maniya	Slightly foliated grey granite intruded by pink granite	
BCTG 14	Near Tatam	Slightly deformed grey granite	
BCTG 26	Maniya	Slightly foliated granite intruded by pink granite	
BSTM 1	Near Khajuraho	Pink granite intruding porphyritic granite	
BSTM 3	Near Khajuraho		

Table 2: Continued.

Sample no.	Location	Description	Mineralogy
BSTM 104*	Khajuraho	Cross-cutting dykes with numerous mafic enclaves, intruded by HSLM monzogranites	
BE 39	Khajuraho	Slightly mafic granitoids cut by porphyritic granites	
BE 40	Khajuraho	Slightly mafic granitoids cut by porphyritic granites	
BSTG 108*	Karara, near Mahoba	Dark grey granitoids intruding 3.3 Ga TTGs	
BSTG 119*	Karera	Dark grey homogeneous intrusions with slight gneissic appearance at places intruded by pegmatites	
BSTG 120*	Near Raksa	Dark grey deformed granitoids with high migmatisation at places	
BSTG 131*	Near Karera Fort	Dark grey deformed granitoids showing gneissic banding	
BSTG 9	Lakshmanpura mines	Dark grey granites intruded by pegmatites and aplite veins	
BC.35	Kochabhawar, Jhansi	Large sanukitoids outcrop from the Kochabhawar, intruded by anatectic granites	Plg (55%), Hbl (16%), Qtz (15%), Bt (8%), and Kfs (5%); accessory phases: zircon, titanite, apatite, and opaque minerals
BC16-18	Sakrar	Grey to light grey, moderate to crudely foliated outcrops locally containing mafic minerals in aggregates or clots	
BC16-01	Jhansi		
BC16-03	Shankargarh		
High silica low magnesium granitoids/anatectic granites			
BLHM 118*	Raksa	Medium- to coarse-grained grey granites with mafic magmatic enclaves	
BLHM 127*	Garmau	Grey granites with mafic magmatic enclaves showing flow structures at places	
BLHM 27	Mahoba-Chatarpur road	Grey granite in contact with gneiss	
BLHM 21	Tatam	Pink granite in contact with slightly deformed grey granite	
BLHM 28	Near Malhara	Massive porphyritic pink granite	
BLHM 20	Bukhara Gaon	Massive porphyritic grey granite	
BLHM 126	Rund Karari quarry	Massive grey granites intruded by pink granite	
BLEM 102	Mundara, Jaawan	Grey porphyritic granites with phenocryst of feldspar	Kfs (~35 vol%), Qtz (~40 vol%), Pl (~22 vol%), and Bt (~2 vol%) with accessory phases like amphibole, titanite, epidote, apatite, and zircon (~1 vol%)
BLEM109*	Talbehat	Porphyritic grey to pink granites showing rapakivi texture	
BLEM 124*	Sukwa Dukwa, Babina	Porphyritic granites showing rapakivi texture (locally) and intruding TTGs	
BLEM 30	Rampura quarry	Massive relatively undeformed grey granite	
BLEM 11	Near Mauranipur	Porphyritic grey granite	
BMG 105*	Near Khajuraho	Massive pink colored undeformed granites	
BMG 113	Rund Karari quarry	Pink granite intruding massive grey granite	
BMG 130*	Bijoli quarry	Grey granites with occasional presence of xenoliths	
BMG 41	Kabrai	Grey granite intruded by pegmatites and aplite veins	

Table 2: Continued.

Sample no.	Location	Description	Mineralogy
BMG 14	Bijoli	Undeformed grey granite	
BMG 9	Maniya	Pink granite intruding slightly deformed grey granite	
BC.33	Baghora, Babina	Medium- to fine-grained, undeformed granites locally containing xenoliths of TTG and granodiorites.	Kfs (38–39%), Qtz (32–33%), Pl (21–22%), and Bt (4–5%) with some accessory minerals such as zircon, titanite, and apatite

Sources: Joshi et al. [9, 40]; Joshi and Slabunov [53]; Singh et al. [50], [43]; this study. *The U-Pb zircon ages of these samples can be found in Joshi et al. [9].

Figure 3: (a) Migmatised TTGs exposed near Babina; (b) relatively homogeneous TTGs exposed near Mauranipur; (c, d) LSHM granitoids exposed near Orchha and Karera; (e) HSLM anatectic pink granite exposed near Khajuraho; (f) HSLM porphyritic granites exposed near Talbehat.

Archaean-Proterozoic boundary. The multicationic classification diagram [73], $Al_2O_3/(FeO_t+MgO)$, $3 * CaO$, $5 * (K_2O/Na_2O)$, and $2 * A/CNK$; Na_2O/K_2O ratio; and $2 * (FeO_t + MgO)$ wt% $*$ (Sr + Ba) wt%(=FMSB) diagrams [10] for the Bundelkhand granitoids are shown in Figure 6. The TTGs plot in the tonalite and granodiorite fields, whereas the LSHM sanukitoids and hybrids mainly occupy the granodiorite, quartz monzonite, and granite fields (Figure 6(a)). The anatectic HSLM group falls in the quartz monzonite and granite fields (Figure 6(a)). Figure 6(b) shows that the major-element composition of LSHM sanukitoids and hybrid granitoids does not point to an origin through the melting of a single crustal lithology. Several studies have proposed a mixed origin, viz., mixing between sanukitoid and TTGs, contamination of juvenile magma with preexisting crust, and mixing of TTG magma with enriched mantle, for such granitoids [9, 74–76]. On plotting the studied granitoids on the Na_2O/K_2O-FMSB-A/CNK plot (Figure 6(c)), it is noted that the studied granitoids fall well within TTG, sanukitoid, hybrid granitoid and biotite, and two mica granites from the Dharwar craton.

The change from sodic TTGs to potassic granodiorites and granites is considered to be a consequence of increasing crustal contributions. In addition to the composition of the granitoids, certain geochemical fingerprints, differences in U-Pb zircon formation ages and Nd model ages, $\varepsilon Nd(t)$ values, and occurrence of inherited zircons are regarded as measures of crustal contamination. In this discussion, we compare the main geochemical signatures of the Bundelkhand granitoids with Nd results (Appendix 1) of this and other relevant studies from the Dharwar and Aravalli cratons [43, 44, 77–84]. To study the sources of granitoids, the selected elements [SiO_2, Na_2O, K_2O, MgO, P_2O_5, Ba +Sr, and $(Gd/Er)_N$] are plotted against U-Pb zircon ages (Figures 7 and 8) and $\varepsilon Nd(t)$ values (Figures 9 and 10). The SiO_2 and MgO contents reflect the mantle vs. crust

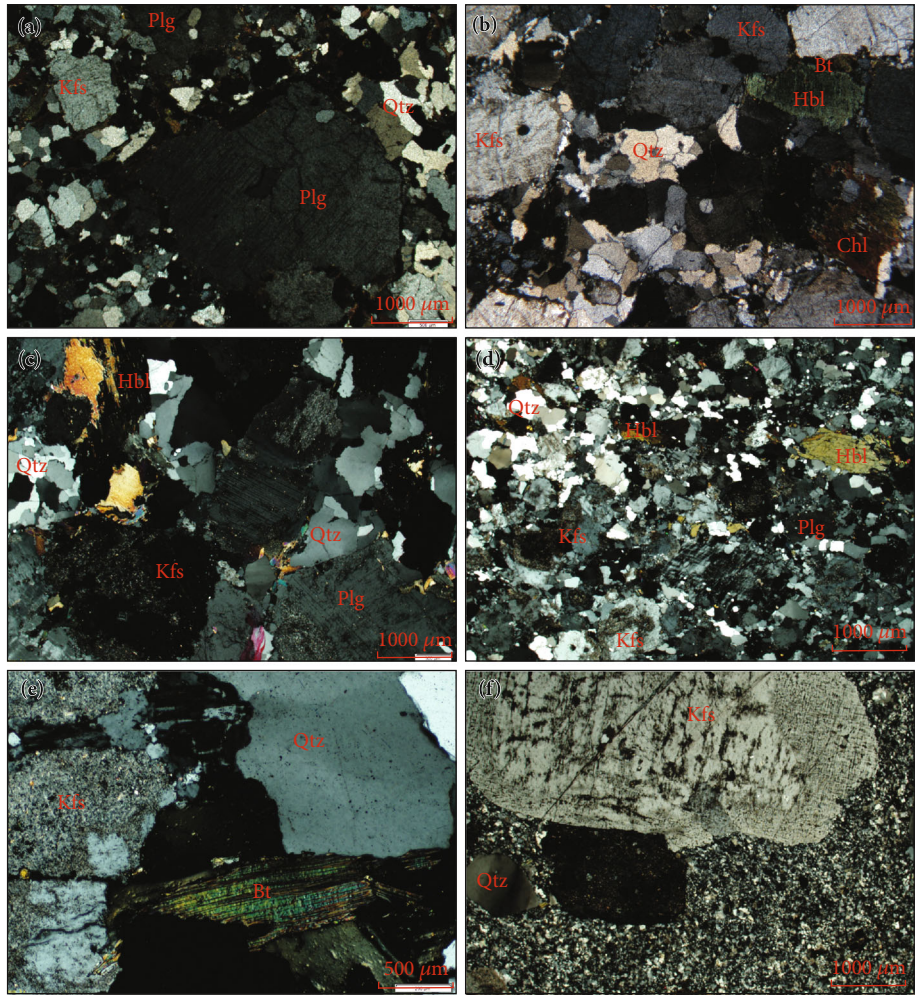

Figure 4: Photomicrographs of TTGs (a, b), LSHM (c, d), and HSLM (e, f) granitoids from the Bundelkhand craton.

contributions, Na_2O indicates the role of a basaltic source, K_2O may indicate crustal contamination or origin from an enriched mantle, and P_2O_5 and Ba+Sr are regarded as indicators of contributions from an enriched mantle.

6.1. Geochemical vs. Neodymium Isotope Signatures

6.1.1. Tonalite-Trondhjemite-Granodiorites (TTGs). The Bundelkhand TTGs carry the specific "basaltic crust signature" typical for Archaean TTGs: high Na and SiO_2 contents and low contents of mantle compatible elements. The number of samples is not adequate for far-reaching interpretations but allows us some conclusions on the TTGs of the Bundelkhand craton. The element vs. U-Pb zircon age plots (Figure 7) indicate that the Paleoarchaean TTGs (3.3-3.2 Ga) show a wider range in their SiO_2 and MgO contents than the Neoarchaean TTGs (2.7 Ga). Table 4 shows that the Paleoarchaean TTGs have shorter time gaps (~41-220 Ma) between the U-Pb formation ages and Nd model ages than the Neoarchaean TTGs (~354-601 Ma). For the Paleoarchaean TTGs, the element vs. $\varepsilon Nd(t)$ plot (Figure 9) shows a narrow range of slightly positive $\varepsilon Nd(t)$ values between 1.96 and -0.53, but there is no correlation between the SiO_2 or MgO contents and $\varepsilon Nd(t)$ values. Conversely, Neoarchaean TTGs show mainly negative and more variable $\varepsilon Nd(t)$ values (between -2.61 and 0.36). The increasing SiO_2 and slightly falling MgO trends with decreasing $\varepsilon Nd(t)$ values (Figure 9) point towards derivation from a mafic crust contaminated by preexisting crust.

Figure 7(g) shows that Paleoarchaean TTGs have variable HREE characteristics, as measured by the $(Gd/Er)_N$ ratio, whereas the Neoarchaean samples show high HREE characteristics. The reason for the variation in the HREE contents of TTGs is not sustained yet, but melting at different depths can account for the variation [28, 85, 86]. In the Bundelkhand craton, the high-HREE TTGs occur as metatexite enclaves in diatexitic low-HREE TTGs. This may indicate migration of melts from deep garnet-bearing sources into garnet-free amphibolite facies as suggested for TTGs of Arctic Fennoscandia [28]. Short time gaps between formation and model ages, narrow range of slightly positive $\varepsilon Nd(t)$ values, and wide variation of SiO_2 and MgO

Table 3: Isotopic data for TTGs and high-K granitoids from the Bundelkhand craton.

Name	Age (Ma)	Sm	Nd	$^{147}Sm/^{144}Nd$	$^{143}Nd/^{144}Nd$	$^{143}Nd/^{144}Nd$ (i)	$\varepsilon Nd(t)$	T_{DM1} (Ma)	T_{DM2} (Ma)	Sm/Nd
TTGs										
BETTG 107*	3335	14.37	73.72	0.1183	0.511008	0.508400	1.96	3156	3397	-0.40
BETTG 1	3435	2.63	15.39	0.1037	0.510605	0.508249	1.57	3284	3500	-0.47
BETTG 5	3335	2.99	14.87	0.1218	0.511062	0.508376	1.48	3187	3440	-0.38
BETTG 9	3335	7.06	35.73	0.1198	0.511017	0.508374	1.44	3193	3440	-0.39
BETTG 3	3335	5.11	26.60	0.1166	0.510922	0.508351	0.99	3230	3472	-0.41
BETTG 11*	3435	4.64	23.92	0.1178	0.510872	0.508197	0.54	3340	3592	-0.40
BLHTTG 2	2713	3.34	20.32	0.0996	0.510919	0.509135	0.36	2783	2965	-0.49
BLHTTG 1*	2713	3.65	19.73	0.1124	0.511099	0.509088	-0.57	2858	3067	-0.43
BLHTTG 4	2713	5.01	27.32	0.1113	0.511022	0.509030	-1.71	2936	3147	-0.43
BLHTTG 3	2713	2.71	15.58	0.1057	0.510916	0.509023	-1.84	2934	3134	-0.46
BLHTTG 7	2713	3.70	17.53	0.1282	0.511278	0.508984	-2.61	3053	3314	-0.35
LSHM										
BCTG 129*	2554	3.59	19.96	0.1091	0.510980	0.509142	-3.60	2937	3144	-0.45
BCTG 101	2554	5.90	37.46	0.0955	0.510906	0.509297	-0.54	2707	2878	-0.51
BCTG 27	2539	5.19	37.64	0.0837	0.510906	0.509504	3.13	2475	2619	-0.57
BCTG 14	2539	4.66	32.10	0.0882	0.510906	0.509429	1.66	2559	2712	-0.55
BCTG 26	2539	4.92	35.29	0.0846	0.510906	0.509489	2.84	2492	2638	-0.57
BSTM 1	2539	5.38	36.34	0.0898	0.510670	0.509167	-3.49	2861	3032	-0.54
BSTM 3	2539	8.40	53.31	0.0956	0.510781	0.509180	-3.24	2861	3040	-0.51
BSTM 104*	2539	5.60	38.18	0.0890	0.510675	0.509185	-3.12	2838	3007	-0.55
BE 39	2539	8.52	62.05	0.0833	0.510636	0.509242	-2.02	2764	2921	-0.58
BE 40	2539	12.54	83.09	0.0916	0.510750	0.509216	-2.53	2809	2979	-0.53
BSTG 108*	2578	6.77	40.93	0.1003	0.510878	0.509172	-2.38	2850	3036	-0.49
BSTG 119*	2563	4.40	25.07	0.1066	0.510953	0.509151	-3.18	2908	3108	-0.46
BSTG 120*	2559	3.92	24.57	0.0967	0.510882	0.509250	-1.33	2762	2938	-0.51
BSTG 131*	2559	3.45	24.41	0.0858	0.510721	0.509274	-0.87	2719	2878	-0.56
BSTG 9	2563	3.99	22.28	0.1086	0.511056	0.509220	-1.82	2820	3019	-0.45
HSLM										
BLHM 118*	2562	2.10	19.80	0.0644	0.510372	0.509285	-0.59	2686	2820	-0.67
BLHM 127*	2552	3.45	33.77	0.0619	0.510219	0.509176	-2.97	2791	2927	-0.69
BLHM 27	2565	5.55	39.13	0.0860	0.510559	0.509104	-4.05	2906	3074	-0.56
BLHM 21	2555	2.46	15.26	0.0978	0.510894	0.509247	-1.51	2772	2950	-0.50
BLHM 28	2562	6.37	48.72	0.0794	0.510590	0.509249	-1.29	2737	2889	-0.60
BLHM 20	2562	2.32	15.76	0.0893	0.510709	0.509201	-2.24	2806	2973	-0.55
BLHM 126	2552	4.97	41.98	0.0719	0.510417	0.509207	-2.37	2776	2921	-0.63
BLEM 102	2589	6.12	38.47	0.0965	0.510843	0.509195	-1.65	2806	2983	-0.51
BLEM109*	2544	11.47	75.71	0.0919	0.510806	0.509265	-1.44	2749	2917	-0.53
BLEM 124*	2546	9.85	68.54	0.0872	0.510758	0.509294	-0.82	2707	2867	-0.56
BLEM 30	2546	11.81	79.23	0.0904	0.510554	0.509035	-5.89	3010	3190	-0.54
BLEM 11	2565	9.59	59.56	0.0977	0.510864	0.509211	-1.95	2807	2987	-0.50
BMG 105*	2565	3.19	20.38	0.0951	0.510902	0.509294	-0.33	2703	2873	-0.52
BMG 113	2565	4.16	24.86	0.1016	0.510937	0.509218	-1.81	2806	2992	-0.48
BMG 130*	2555	4.01	28.16	0.0864	0.510656	0.509200	-2.43	2806	2969	-0.56
BMG 41	2555	4.28	29.67	0.0876	0.510666	0.509191	-2.61	2819	2984	-0.55
BMG 14	2565	2.44	15.55	0.0952	0.510906	0.509295	-0.30	2701	2871	-0.52
BMG 9	2565	8.06	42.50	0.1150	0.511121	0.509176	-2.65	2898	3115	-0.42

*U-Pb ages from Joshi et al. [9] and unpublished data.

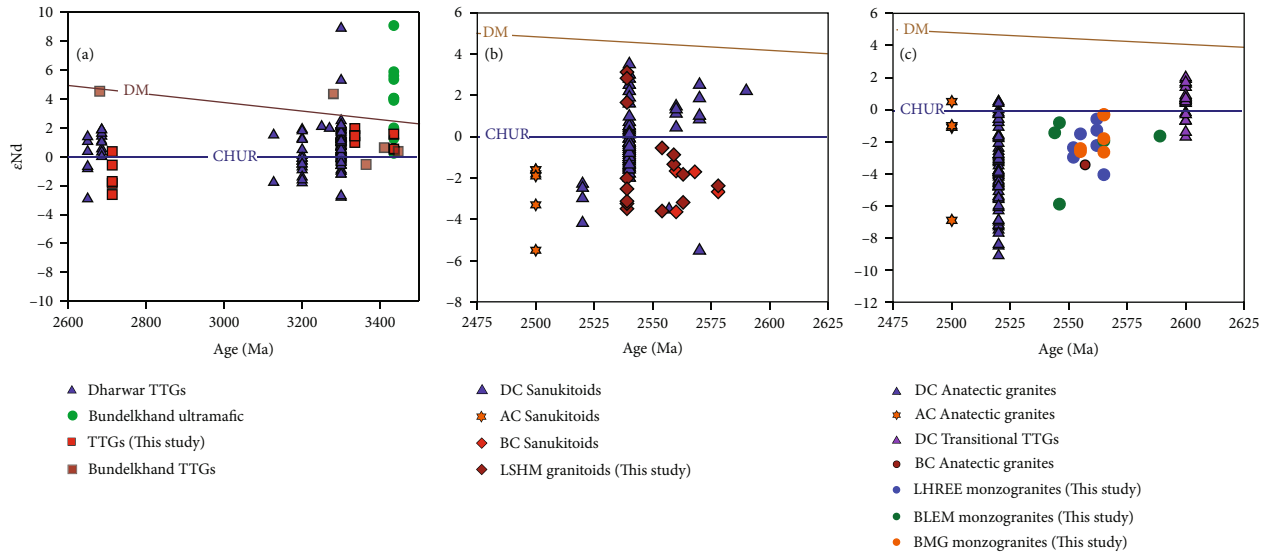

Figure 5: $\varepsilon Nd(t)$ vs. time (zircon ages) evolution diagram for TTG, LSHM (sanukitoid and hybrid), and HSLM granitoids from the Bundelkhand, Aravalli, and Dharwar cratons. Data are from this study and previous studies [43, 44, 77, 78, 80, 83, 104, 105].

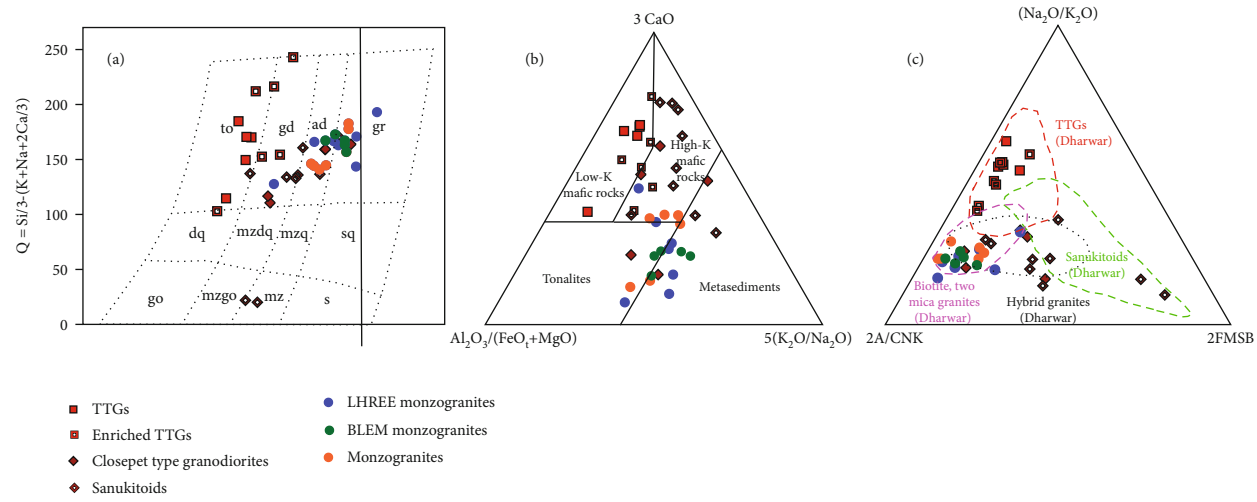

Figure 6: (a) Multicationic classification diagram for Bundelkhand granitoids (after [73]). Abbreviations: to: tonalite; gd: granodiorite; ad: quartz monzonite; gr: granite; dq: quartz diorite; mzdq: quartz monzodiorite; mzq: quartz monzonite; sq: quartz syenite; go: gabbro; mzgo: monzogabbro; mz: monzonite; s: syenite. (b) Ternary diagram $Al_2O_3/(FeO_t+MgO)$; $3 * CaO$; $5 * (K_2O/Na_2O)$ for Bundelkhand granitoids (after [10]). (c) Ternary classification diagram for late-Archaean granitoids: $2 * A/CNK$ (molar $Al_2O_3/[CaO+Na_2O+K_2O]$ ratio); Na_2O/K_2O ratio; $2 * (FeO_t + MgO)$wt.% $* (Sr + Ba)$wt.% (=FMSB) (after [10]).

lacking correlation with $\varepsilon Nd(t)$ values suggest that the Paleoarchaean TTGs formed from juvenile of short-lived mafic crust with contributions from newly formed felsic crust wherein distinct isotope compositions had not developed yet. In the Neoarchaean TTGs, long gaps between formation and model ages as well as SiO_2 and MgO correlating with negative $\varepsilon Nd(t)$ values indicate interactions of juvenile sources with older sources. The presence of inherited zircons in ~2.70 Ga TTGs [43] further supports our conclusion.

Based on the above, we conclude that the geochemical and Nd isotope signatures of Archaean Bundelkhand TTGs point towards partial melting of juvenile or short-lived mafic crust at different depths with variable contributions from newly formed felsic crust in the Paleoarchaean and older felsic crust in the Neoarchaean. This may reflect the transition from melting in Paleoarchaean oceanic plateau in plume settings to shallow melting in Neoarchaean subduction-related island arcs.

6.1.2. High-K LSHM Sanukitoids and Hybrids. The LSHM granitoids, especially sanukitoids, carry a specific "enriched mantle signature" (high Mg-K-Ba-Sr-P and LREE) that is inherited from Archaean mantle overprinted by crust-

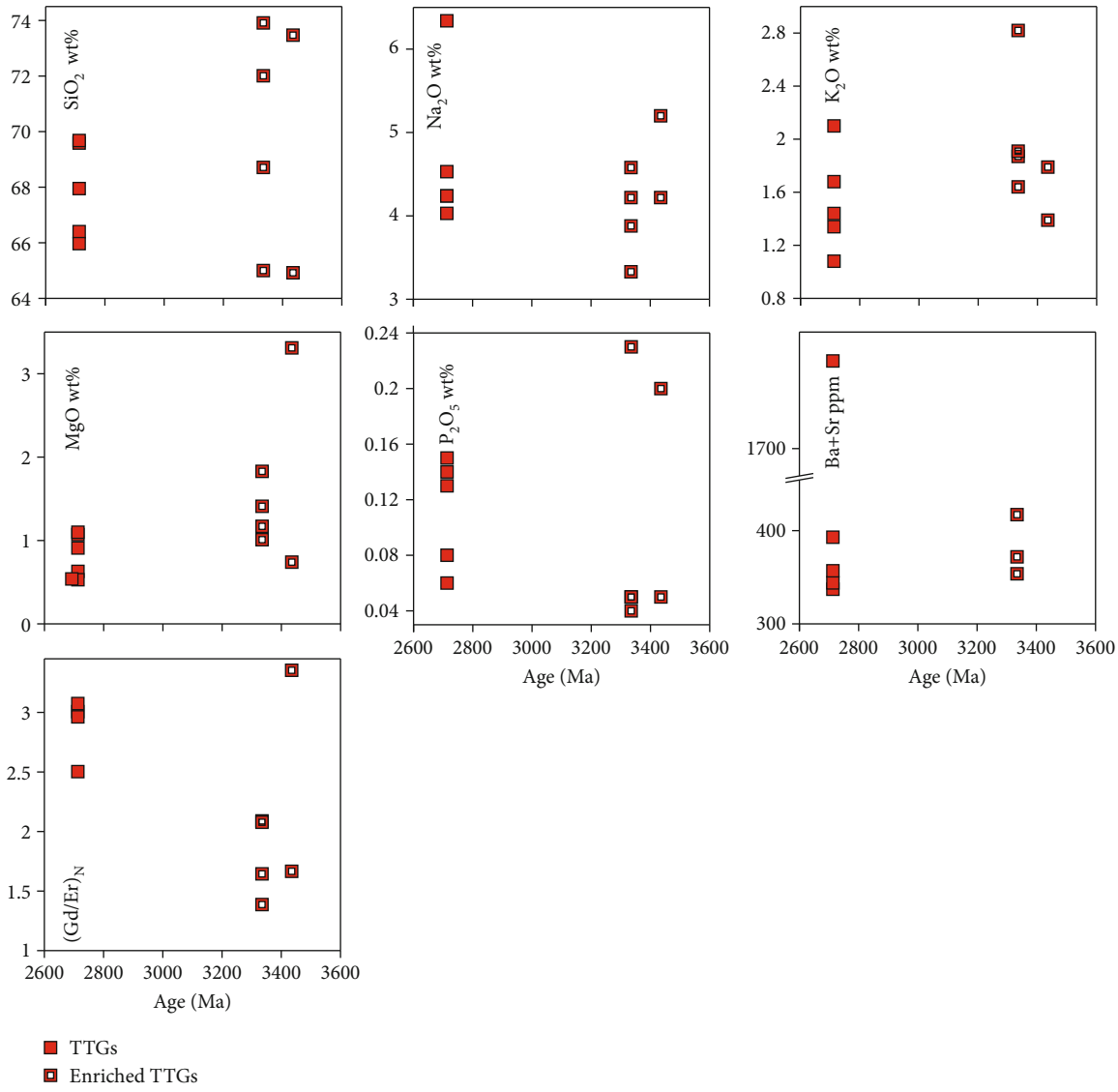

Figure 7: Selected elements vs. U-Pb zircon formation age for TTGs of the Bundelkhand craton.

mantle interactions. This signature cannot be a consequence of fractional crystallization, because it is independent of the SiO_2 content and occurs in mafic rocks, such as lamprophyres, which are often associated with sanukitoids.

The element vs. U-Pb zircon age plots (Figure 8) indicate that the 2.5 Ga LSHM granitoids have a wider range of element contents than the HSLM group of granitoids. The LSHM granitoids show variable time gaps (~99-590 Ma) between the U-Pb formation age and Nd model age (Table 4). The $\varepsilon Nd(t)$ values for the LSHM group consisting of sanukitoid and hybrid granitoids range from -3.64 to 3.13 (Table 4). Sanukitoids show a narrow range of $\varepsilon Nd(t)$ values and wide variation in Na_2O, K_2O, MgO, P_2O_5, $(Gd/Er)_N$, and high Ba+Sr contents but a minor variation in the SiO_2 content (Figure 10). Some of the hybrid granitoids show higher $\varepsilon Nd(t)$ values than sanukitoids. Those with positive $\varepsilon Nd(t)$ values show mainly higher SiO_2 content and lower MgO content, which supports crustal assimilation. Other signatures are similar to those of sanukitoids.

The enriched mantle geochemical signature (high Mg-K-Ba-Sr-P) is typical for sanukitoid granitoids. The plots in Figure 10 show that these elements do not correlate with SiO_2 content or $\varepsilon Nd(t)$ values; therefore, we agree that the signature comes from an enriched mantle. Our results support the previous ideas on the enrichment of the mantle by partial melting in a mantle wedge [87–89] metasomatized by slab-derived melts or fluids from a subducting oceanic slab [87, 90, 91]. Two-stage enrichment, firstly by subduction and secondly by low-degree melting and metasomatism in the mantle would best explain the lack of correlation between Nd isotope and geochemical signatures [85]. Some researchers [92–94] have suggested that sanukitoids were formed by interactions between mantle and TTG melts. However, the discrepancy between ages as well as geochemical and Nd isotope signatures contradicts this suggestion in the Bundelkhand craton. According to Halla [95], radiogenic Pb isotope signatures that developed in the old preexisting crust may erode and enter the mantle, overprint the mantle

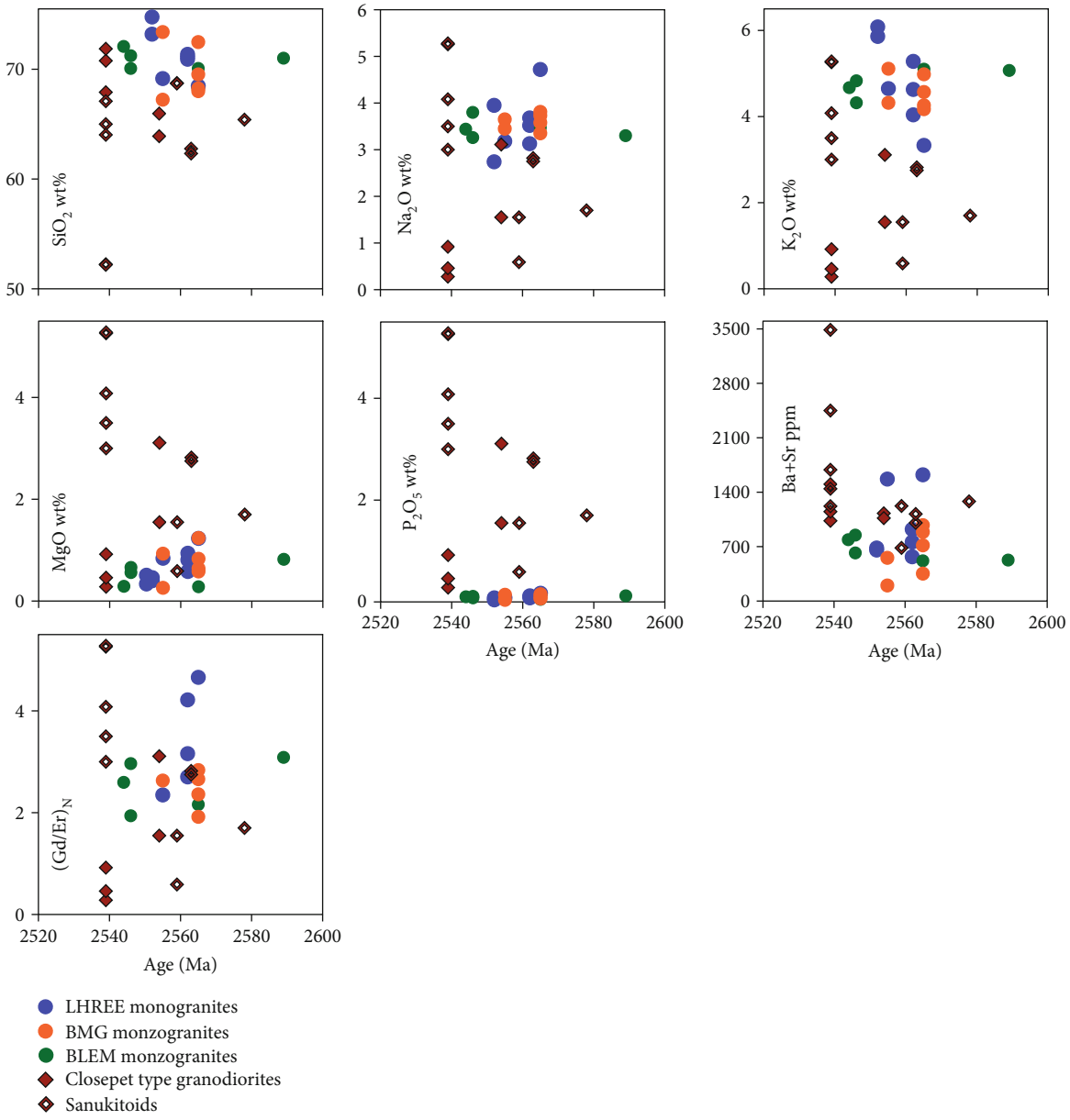

Figure 8: Selected elements vs. U-Pb zircon formation age for high-K granitoids of the Bundelkhand craton.

composition, and return to the crust by juvenile magmatism. Such crustal isotope signatures in mantle-derived rocks form proof of crustal recycling and subduction processes. This implies that crustal signatures may be observed in geochemistry but not in the isotope systematics (in the case of young crust) and vice versa (in the case where crustal isotope signatures are inherited from the mantle).

6.1.3. High-K HSLM Anatectic Group. The HSLM anatectic granitoids show a "continental crust signature" (high SiO_2 and K_2O contents, mantle and enriched mantle signatures absent) pointing to pure crustal origin. The element vs. U-Pb zircon age plots in Figure 8 show less variation in the element contents than the LSHM group. The time gap between formation and model age varies between 258 and 644 Ma. The $\varepsilon Nd(t)$ values for the HSLM group are all negative and range from -0.30 to -5.89 (Table 4). These values are consistent with the derivation from reworking of a heterogeneous crustal source, pointing to the involvement of older heterogeneous crust. The HSLM group shows a relatively narrow range of $\varepsilon Nd(t)$ values and minor variation in the element contents without correlation with $\varepsilon Nd(t)$ (Figure 10), which supports a pure crustal source without a mantle contribution. The absence of inherited zircon grains in HSLM varieties led Singh et al. [44]) to conclude that these anatectic granitoids were formed in conditions that inhibit zircon survival; however, Joshi et al. [9] reported $^{207}Pb/^{206}Pb$ xenocrystic zircon ages of 3568 Ma and 2787 Ma from HSLM granitoids. The involvement of the crustal component in the generation

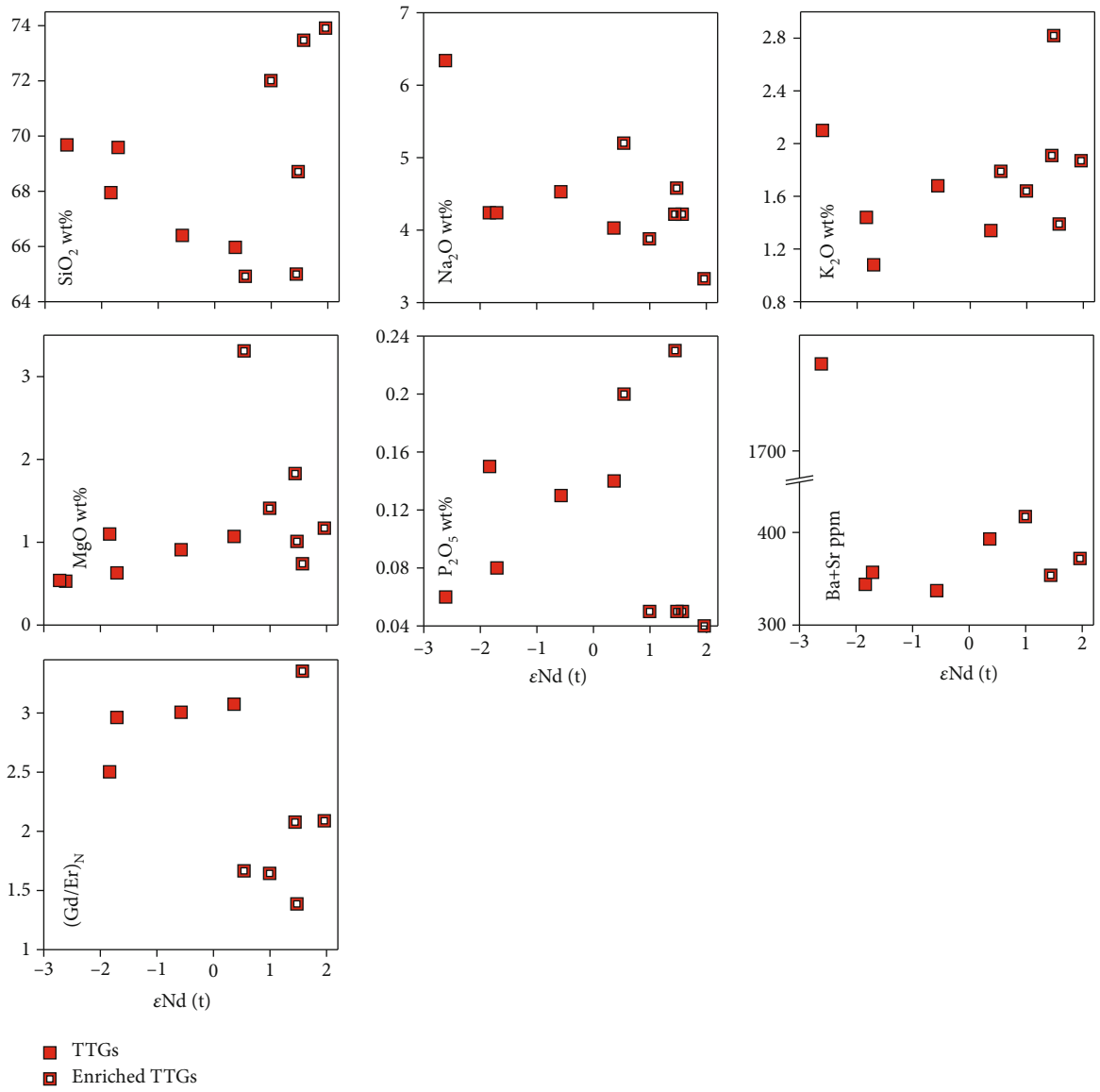

Figure 9: Selected elements vs. $\varepsilon Nd(t)$ diagrams for TTGs of the Bundelkhand craton.

of LSHM as well as HSLM granitoids is further supported by the occurrence of xenocrystic zircons within both the granitoid groups (LSHM and HSLM), which further suggests that crustal reworking was at its peak during the Neoarchaean.

7. Archaean Crustal Evolution

The location of the Indian cratons on a world map modified after Bleeker [96] and the geochronology of TTGs, sanukitoids, and anatectic granitoids in the Bundelkhand, Aravalli, Singhbhum, Bastar, and Dharwar cratons in India are shown in Figure 11. The North China craton is included in the figure because it shows pulses of 2.5 Ga LSHM and HSLM magmatism comparable to the Bundelkhand craton. Next, we describe how the results from the Bundelkhand craton relate to Archaean crustal evolution in general.

7.1. Eoarchaean 4000-3600 Ma. In the Eoarchaean, TTGs with high SiO_2, high Na, MgO, and variable HREE formed by episodic melting within the thin or thickened basaltic crust. Eoarchaean ages have not been reported in the Bundelkhand craton, but the oldest documented U-Pb ages of 3.55 Ga for zircons and 3.59 Ga for zircon xenocrysts together with the oldest model ages of 3592 Ma suggest that the crust formation in the craton started close to the Eoarchaean-Paleoarchaean boundary [54, 58]. Eoarchaean TTGs are found, for example, in the Slave Province, West Greenland, and North China craton.

7.2. Paleoarchaean 3600-3200 Ma. In the Paleoarchaean, TTG magmatism continued along with the formation of diorites and anatectic high-K granites. The Singhbhum and West Dharwar cratons show abundant TTG formation in the Paleoarchaean, and the Bundelkhand craton includes abundant rafts of Paleoarchaean TTGs. The geochemical

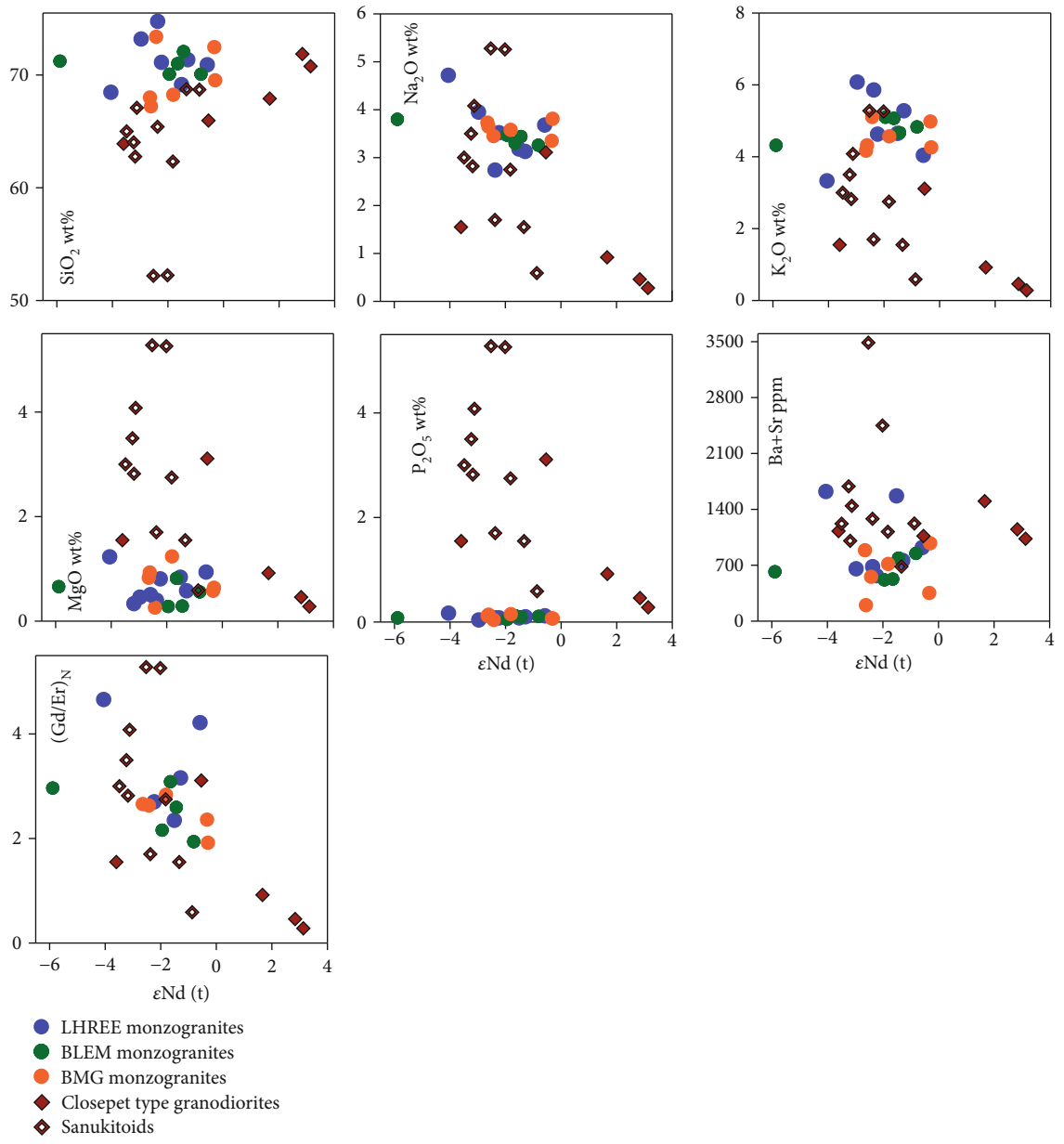

Figure 10: Selected elements vs. $\varepsilon Nd(t)$ diagrams for high-K granitoid of the Bundelkhand craton.

and Nd isotope signatures of 3.4-3.2 Ga Bundelkhand TTGs point towards partial melting of juvenile or short-lived mafic crust at different depths (reflected by variable $(Gd/Er)_N$ ratios) with some crustal contributions. Paleoarchaean TTG crust shows slightly positive $\varepsilon Nd(t)$ values that do not correlate with crustal geochemical signatures. The time gaps between crystallization and model ages are short. These indicate contributions from a newly formed crust that has not yet developed a distinct isotope composition. Figure 11 shows that in India, especially the Bundelkhand, Singhbhum, and Western Dharwar cratons were active during the Paleoarchaean. Figure 5 shows that the $\varepsilon Nd(t)$ values from the Bundelkhand craton are comparable to those from the Dharwar craton.

7.3. Mesoarchaean 3200-2800 Ma. In the Mesoarchaean, the TTG formation continued, but the Bundelkhand craton was quieter until the Neoarchaean. The first LSHM sanukitoid granitoids appeared at 3.0 Ga in the Carajas Province, Brazil [92, 93] and the Pilbara craton, Australia [97]; however, no such granitoids have been reported from the Bundelkhand craton.

7.4. Neoarchaean 2800-2500 Ma. In the early Neoarchaean, 2.7 Ga TTG crust shows negative $\varepsilon Nd(t)$ values that correlate with crustal geochemical signatures. The long gaps between the crystallization and model ages indicate significant contributions from the older crust. These discoveries may reflect the transition from the Paleoarchaean primitive oceanic

Table 4: Representative geochemical data for Bundelkhand granitoids.

Sample no.	Latitude/longitude		SiO_2	MgO	Ba+Sr	εNd(*t*)	Age (Ma)	TDM (Ma)
TTGs								
BLHTTG 4*/BTTG 123	N 25°11′20.8″	E 78°28′33.7″	66.40	0.91	337	-0.57	2713	3067
BLHTTG 2	N 25°12′01.1″	E 78°30′57.8″	65.97	1.07	393	0.36	2713	2965
BLHTTG 3	N 25°12′01.1″	E 78°30′57.8″	67.95	1.10	344	-1.84	2713	3134
BLHTTG 1	N 25 11′20.8″	E 78°28′3.7″	69.59	0.63	357	-1.71	2713	3147
BLHTTG 7	N 25°13′20.7″	E 78°28′04.1″	69.68	0.53	1738	-2.61	2713	3314
BETTG 1	N 25°11′05.5″	E 79°6′24.4″	73.47	0.74	501	1.57	3435	3500
BETTG 107*	N 25°19′49.3″	E 79°49′04.0″	73.91	1.17	372	1.96	3335	3397
BETTG 11*/BETTG 133	N 25°13′7.28″	E 79°05′56.55″	_	_	474	0.54	3435	3592
BETTG 3	N 25°19′49″	E 79°49′4.2″	72.01	1.41	418	0.99	3335	3472
BETTG 5	N 25°19′49″	E 79°49′4.2″	68.71	1.01	468	1.48	3335	3440
BETTG 9	N 25°19′49″	E 79°49′4.2″	65.00	1.83	388	1.44	3335	3440
BC.16	N 25°12′44″	E 79°10′10″	73.73	0.44	672	0.63	3410	3451
BC.45	N 25°12′12″	E 79°07′31″	68.82	1.44	488	-0.53	3364	3556
BC.60	N 25°19′48″	E 79°49′03″	72.82	0.51	659	4.33	3280	3060
BC.61	N25°19′48.9″	E 79°49′04.7″	64.84	2.43	275	0.38	3446	3420
BC.27	N 25°12′23″	E 78°27′42″	66.48	1.27	337	4.54	2681	2480
Low silica high magnesium granitoids/sanukitoids								
BCTG 129*	N 25°25′05.5″	E 78°39′05.8″	63.90	1.55	1129	-3.60	2554	3144
BCTG 101	N 25°23′23.3″	E 78°38′34.2″	65.96	3.11	1067	-0.54	2554	2878
BCTG 27	N 25°01′10.5″	E 79°53′38.3″	70.78	0.28	1032	3.13	2539	2619
BCTG 14	N 25°02′49.2″	E 79°51′52″	67.91	0.92	1502	1.66	2539	2712
BCTG 26	N 25°01′10.5″	E 79°53′38.3″	71.86	0.46	1151	2.84	2539	2638
BSTM 1	N 24°52′36.6″	E 79°56′7.3″	65.00	3.00	1220	-3.49	2539	3032
BSTM 3	N 24°52′36.6″	E 79°56′7.3″	64.03	3.50	1689	-3.24	2539	3040
BSTM 104*	N 24°52′33.1″	E 80°03′05.9″	67.09	4.08	1444	-3.12	2539	3007
BE 39	N 24°52′33.1″	E 80°03′05.9″	52.24	5.26	2450	-2.02	2539	2921
BE 40	N 24°52′33.1″	E 80°03′05.9″	52.19	5.28	3488	-2.53	2539	2979
BSTG 108*	N 25°19′49.3″	E 79°49′04.0″	65.41	1.70	1282	-2.38	2578	3036
BSTG 119*	N 25°27′46.4″	E 78°15′27.6″	62.76	2.82	1005	-3.18	2563	3108
BSTG 120*	N 25°27′3.2″	E 78°29′27.7″	68.74	1.55	683	-1.33	2559	2938
BSTG 131*	N 25°27′33.68″	E 78°08′40.89″	68.70	0.59	1222	-0.87	2559	2878
BSTG 9	N 25°24′23.2″	E 78°29′41.02″	64.03	2.75	1097	-1.82	2563	3019
BC.35	N 25°28′07″	E 78°39′35″	72.57	3.00	1144	-1.70	2568	2911
BC16-18	N 25°21′33″	E 78°51′05″	65.89	1.16	698	-2.67	2578*	_
BC16-01	N 25°26′52″	E 78°36′02″	68.15	1.86	1018	-3.64	2560	_
BC16-03	N 25°26′29″	E 78°38′29″	64.46	2.44	1082	-1.66	2560	_
High silica low magnesium granitoids/anatectic granites								
BLHM 118*	N 25°26′37.5″	E 78°26′25.9″	70.91	0.94	923	-0.59	2562	2820

Table 4: Continued.

Sample no.	Latitude/longitude		SiO_2	MgO	Ba+Sr	εNd(*t*)	Age (Ma)	TDM (Ma)
BLHM 127*	N 25°30′34″	E 78°39′16.8″	73.20	0.46	657	-2.97	2552	2927
BLHM 27	N 25°56′22.9″	E 79°35′50.5″	68.47	1.23	1624	-4.05	2565	3074
BLHM 21	N 25°02′49.2″	E 79°51′52″	70.50	0.84	1071	-1.51	2555	2950
BLHM 28	N 25°01′13.2″	E 79°39′29.8″	71.36	0.58	759	-1.29	2562	2889
BLHM 20	N 25°14′15.7″	E 79°11′10.9″	71.13	0.81	569	-2.24	2562	2973
BLHM 126	N 25°31′14.7″	E 78°31′34.5″	74.76	0.40	682	-2.37	2552	2921
BLEM 102	N 25°21′05.4″	E 78°51′36.5″	71.01	0.82	527	-1.65	2589	2983
BLEM109*	N 25°01′30.06″	E 78°25′13.2″	72.08	0.29	789	-1.44	2544	2917
BLEM 124*	N 25°12′01.1″	E 78°30′57.8″	70.08	0.56	848	-0.82	2546	2867
BLEM 30	N 25°24′49″	E 79°44′17.2″	71.23	0.66	619	-5.89	2546	3190
BLEM 11	N 25°12′33.8″	E 79°07′17.2″	70.08	0.28	76	-1.95	2565	2987
BMG 105*	N 25°10′03.3″	E 79°52′38.5″	72.48	0.58	353	-0.33	2565	2873
BMG 113	N 25°31′14.7″	E 78°31′34.5″	68.25	1.24	763	-1.81	2565	2992
BMG 130*	N 25°21′54.3″	E 78°32′49.5″	73.39	0.26	555	-2.43	2555	2969
BMG 41	N 25°23′30.7″	E 79°59′37.7″	67.23	0.93	736	-2.61	2555	2984
BMG 14	N 25°21′52.9″	E 78°32′48.8″	69.53	0.64	975	-0.30	2565	2871
BMG 9	N 25°01′10.5″	E 79°53′38.3″	68.00	0.83	888	-2.65	2565	3115
BC.33	N 25°09′33″	E 78°28′12″	75.38	0.30	268	-3.44	2557	2975

Sources: this study and Joshi et al. [9], Joshi and Slabunov [53], and Singh et al. ([44], [43]). *The U-Pb zircon ages of these samples can be found in Joshi et al. [9].

plateau setting to island arc accretion along an older protocontinent, possibly related to the formation of the supercontinent Kenorland. During the beginning of the Neoarchaean, the TTG formation decreased and high-K magmatism increased indicating a geodynamic change, probably approaching modern-style plate tectonics with the mantle wedge above subduction zones. The Bundelkhand craton was quiet until the Archaean-Proterozoic boundary when the formation of extensive multisource batholiths involving both mantle- and crust-derived materials (LSHM and HSLM granitoids) started. The most important representatives of this event are found in the Bundelkhand and North China cratons [9, 43, 44, 98, 99].

The geochemical and isotope signatures of the 2.5 Ga LSHM granitoid group correspond to major juvenile inputs (high content of mantle compatible elements with or without older crustal components, as reflected by the εNd(*t*) values varying from negative to positive). Sanukitoid granitoids inherited their special signature (high K-Mg-P-Ba-Sr) from the metasomatically enriched mantle, whereas direct crustal contributions have modified the hybrid granitoids. The enriched mantle signatures in the LSHM granitoids have been related to the onset of modern-style plate tectonic processes [12], as recycling of crustal material into the mantle can enrich the subcontinental lithospheric mantle wedge with incompatible elements and crustal isotope signatures, which is generally attributed to subduction. The LSHM sanukitoid and hybrid granitoids formed from crust-enriched mantle reservoirs with or without mixing with anatectic melts. This scenario points to convergent collisional settings. Figure 11 shows that sanukitoid and hybrid granitoids were formed also in the Dharwar and, especially, in the North China craton (for references, see the figure caption). The formation of abundant multisource granitoid batholiths worldwide marks the stabilisation of the supercontinent Kenorland at the Archaean-Proterozoic boundary.

8. Comparison with Hf and Nd Modal Ages for the Bundelkhand Craton

The Bundelkhand craton is a key locality for studies on the abundant multisource granitoid batholiths that stabilised the supercontinent Kenorland by 2.5 Ga. The Nd isotope of this study supports and provides further constraints for the previous observations based on the geochemistry of the craton and supports results from the previous Hf isotope studies [9, 43, 54, 55]. Figure 12(a) shows the geochronology (U-Pb zircon ages as well as Nd and Hf model ages) of the Archaean TTG enclaves across the Bundelkhand craton from west to east in their key localities in Babina, Mauranipur, and Mahoba. The youngest Neoarchaean and oldest Paleoarchaean TTGs are found in the Babina area; however, most of the TTGs are Paleoarchaean (3.6-3.2 Ga). Figure 12(b) shows a similar diagram for sanukitoid and hybrid types of high-K granitoids as well as anatectic granitoids. The figure shows that abundant granitoids formed within a short time span and stabilised the Bundelkhand craton at the end of the Neoarchaean. The range in Hf model ages indicates an

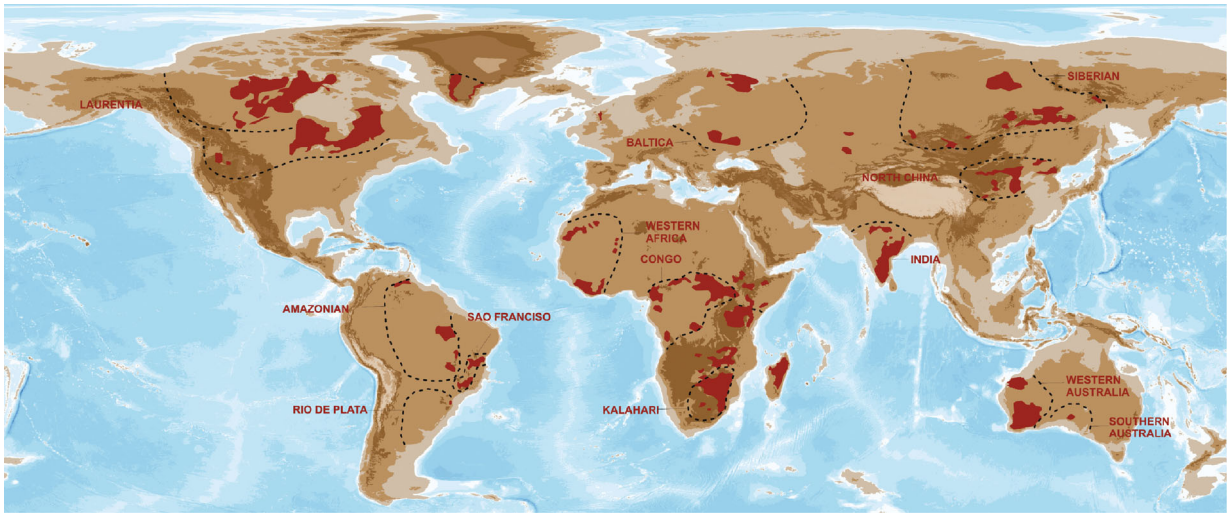

(a)

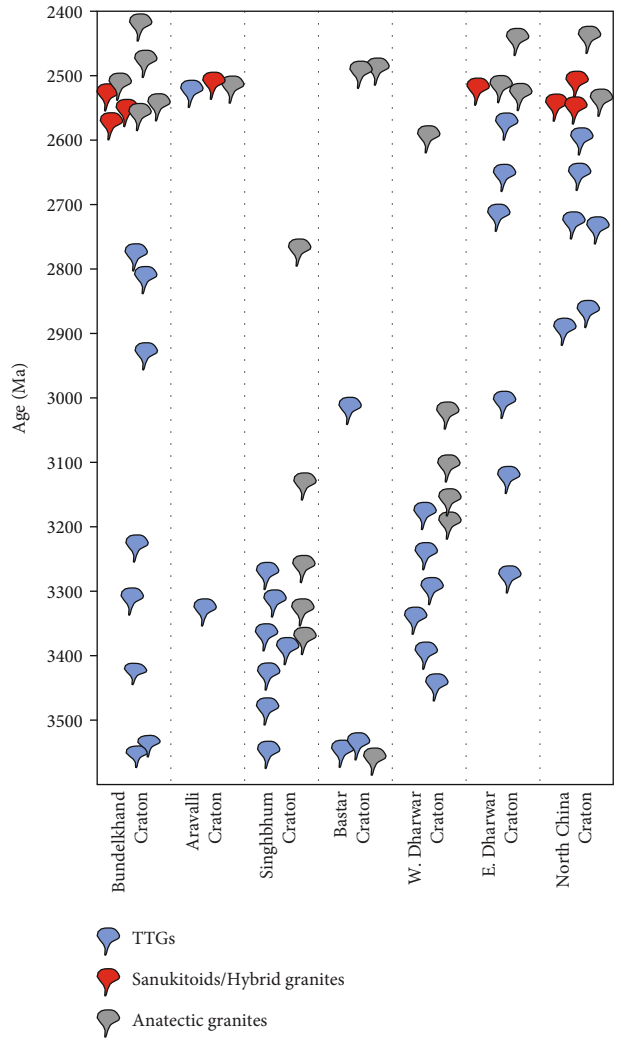

(b)

FIGURE 11: (a) World map showing the distribution of exposed Archaean cratonic blocks, modified after Bleeker [96]. (b) Age distribution of various granitic events in the Dharwar, Bundelkhand, and North China craton (modified and updated from [10, 55]). Additional data sources: Bundelkhand craton [9, 43, 44, 52, 54–58], South India (Dharwar craton and Coorg Block) [80, 81, 104, 106–110], and North China craton [98, 99, 111, 112].

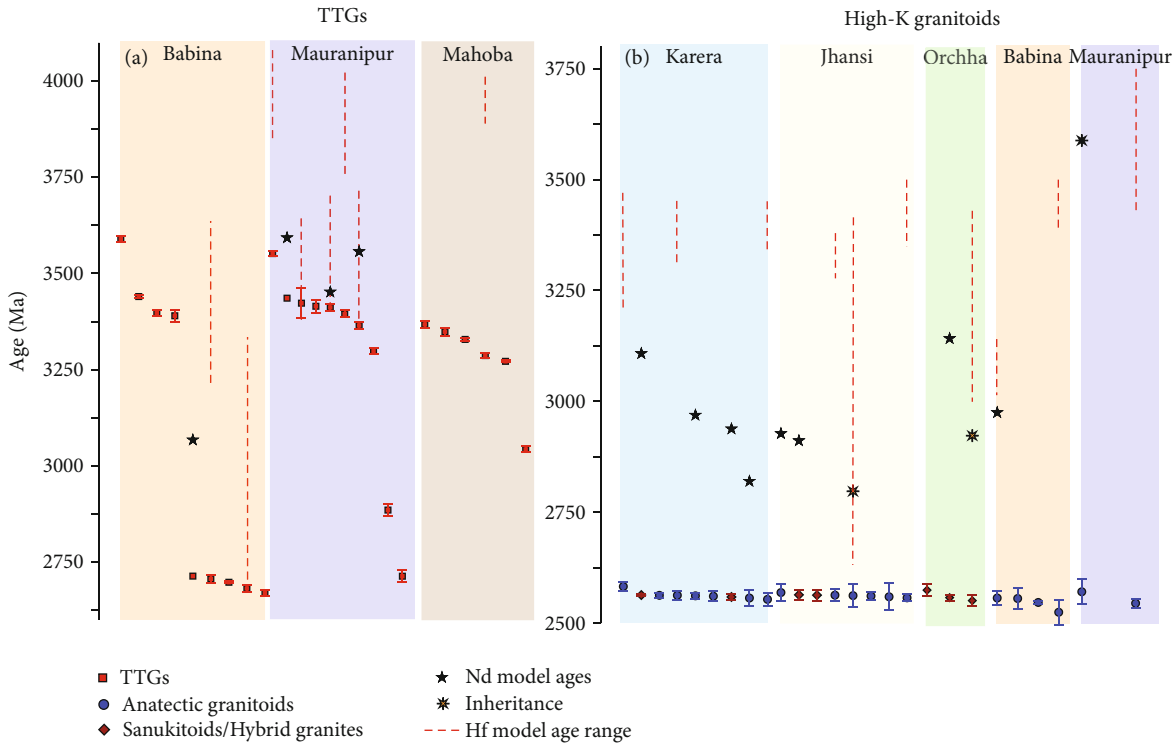

FIGURE 12: Distribution of U-Pb zircon ages and Nd model ages and the range of Hf model ages of the (a) TTGs and (b) high-K (sanukitoids and hybrid) granitoids across the Bundelkhand craton.

inheritance from older sources. For example, the Hf model age range for an anatectic granitoid from Mauranipur is as old as that of the oldest Mauranipur TTGs. This indicates that the high Hf model ages in the high-K granitoids were inherited from the Paleoarchaean TTGs, the sources of the anatectic granitoids. Some Paleoarchaean TTGs may have even inherited Eoarchaean Hf signatures. Overall, the Nd model ages follow the trend of the Hf model ages.

9. Conclusions

Combined geochronology, geochemical signatures, and Nd isotope compositions allow us to draw the following conclusions on the evolution of Archaean granitoids of the Bundelkhand craton:

(1) The geochemical and Nd isotope signatures of Archaean Bundelkhand TTGs point towards partial melting of juvenile or short-lived mafic crust at different depths with contributions from newly formed felsic crust in the Paleoarchaean and older felsic crust in the Neoarchaean. This may reflect the transition from melting in Paleoarchaean oceanic plateaux (3.4-3.2 Ga) in plume settings to shallow melting in Neoarchaean island arcs (2.7 Ga) in subduction settings

(2) The 2.5 Ga high-K granitoids formed at convergent subduction settings by partial melting of the mantle wedge and preexisting crust. Sanukitoids and hybrid granitoids originated in the mantle, the latter showing stronger crustal contributions, whereas abundant anatectic granitoids were the results of the melting of the continental crust

Data Availability

The data used in the manuscript is attached as tables.

Conflicts of Interest

The authors declare that they have no conflicts of interest.

Supplementary Materials

Appendix 1: geochemical data for the studied Archaean granitoids from the Bundelkhand craton. *(Supplementary Materials)*

References

[1] R. N. Mitchell, N. Zhang, J. Salminen et al., "The supercontinent cycle," *Nature Reviews Earth & Environment*, vol. 2, no. 5, pp. 358–374, 2021.

[2] R. D. Nance, J. B. Murphy, and M. Santosh, "The supercontinent cycle: a retrospective essay," *Gondwana Research*, vol. 25, no. 1, pp. 4–29, 2014.

[3] J. J. W. Rogers and M. Santosh, *Continents and Supercontinents*, Oxford University Press, 2004.

[4] H. Martin, J. F. Moyen, M. Guitreau, J. Blichert-Toft, and J. L. Le Pennec, "Why Archaean TTG cannot be generated by MORB melting in subduction zones," *Lithos*, vol. 198-199, pp. 1–13, 2014.

[5] J. van Hunen and A. P. van den Berg, "Plate tectonics on the early earth: limitations imposed by strength and buoyancy of subducted lithosphere," *Lithos*, vol. 103, no. 1-2, pp. 217–235, 2008.

[6] L. Ackerman, J. Žák, V. Kachlík et al., "The diversity of sources of late Archean granites reflects a transition from plume-dominated to plate tectonics in the Superior Province, Canada," *Precambrian Research*, vol. 370, article 106525, 2022.

[7] S. Dey and J.-F. Moyen, "Archean granitoids of India: windows into early Earth tectonics–an introduction," *Geological Society, London, Special Publications*, vol. 489, no. 1, 2020.

[8] J. Halla, M. J. Whitehouse, T. Ahmad, and Z. Bagai, "Archaean granitoids: an overview and significance from a tectonic perspective," *Geological Society Special Publication*, vol. 449, no. 1, pp. 1–18, 2017.

[9] K. B. Joshi, J. Bhattacharjee, G. Rai et al., "The diversification of granitoids and plate tectonic implications at the Archaean-Proterozoic boundary in the Bundelkhand craton, central India," *Geological Society Special Publication*, vol. 449, pp. 123–157, 2017.

[10] O. Laurent, H. Martin, J. F. Moyen, and R. Doucelance, "The diversity and evolution of late-Archean granitoids: evidence for the onset of "modern-style" plate tectonics between 3.0 and 2.5 Ga," *Lithos*, vol. 205, pp. 208–235, 2014.

[11] J.-F. Moyen, "Archean granitoids: classification, petrology, geochemistry and origin," *Geological Society, London, Special Publications*, vol. 489, no. 1, p. 15, 2019.

[12] J. Halla, "Highlights on geochemical changes in Archaean granitoids and their implications for early earth geodynamics," *Geosciences (Switzerland)*, vol. 8, no. 9, p. 353, 2018.

[13] E. Heilimo, P. Mikkola, and J. Halla, "Age and petrology of the Kaapinsalmi sanukitoid intrusion in Suomussalmi, eastern Finland," *Eastern Finland: Bulletin of the Geological Society of Finland*, vol. 79, no. 1, pp. 117–125, 2007.

[14] J.-F. Moyen and O. Laurent, "Archaean tectonic systems: a view from igneous rocks," *Lithos*, vol. 302-303, pp. 99–125, 2018.

[15] S. Ray, K. B. Joshi, S. Sundarraman, D. Joshi, and T. Ahmad, "Geochemical and petrogenetic study of Proterozoic Sewariya and Govindgarh granitoids from South Delhi Fold Belt," *Current Science*, vol. 109, no. 8, p. 1458, 2015.

[16] J. H. Bédard, "Stagnant lids and mantle overturns: implications for Archaean tectonics, magmagenesis, crustal growth, mantle evolution, and the start of plate tectonics," *Geoscience Frontiers*, vol. 9, no. 1, pp. 19–49, 2018.

[17] M. S. Drummond and M. J. Defant, "A model for Trondhjemite-Tonalite-Dacite Genesis and crustal growth via slab melting: Archean to modern comparisons," *Journal of Geophysical Research*, vol. 95, no. B13, pp. 21503–21, 521, 1990.

[18] S. Foley, M. Tiepolo, and R. Vannucci, "Growth of early continental crust controlled by melting of amphibolite in subduction zones," *Nature*, vol. 417, no. 6891, pp. 837–840, 2002.

[19] C. J. Hawkesworth, P. A. Cawood, B. Dhuime, and T. I. S. Kemp, "Earth's continental lithosphere through time," *Annual Review of Earth and Planetary Sciences*, vol. 45, no. 1, pp. 169–198, 2017.

[20] J. E. Hoffmann, C. Zhang, J.-F. Moyen, and T. J. Nagel, "The formation of tonalites–trondjhemite–granodiorites in early continental crust," in *Earth's oldest rocks*, Elsevier Amsterdam, 2019.

[21] J. G. Arth and G. N. Hanson, "Quartz diorites derived by partial melting of eclogite or amphibolite at mantle depths," *Contributions to Mineralogy and Petrology*, vol. 37, no. 2, pp. 161–174, 1972.

[22] H. Martin and J. F. Moyen, "Secular changes in tonalite-trondhjemite-granodiorite composition as markers of the progressive cooling of Earth," *Geology*, vol. 30, no. 4, pp. 319–322, 2002.

[23] J. E. Hoffmann, C. Münker, T. Næraa et al., "Mechanisms of Archean crust formation inferred from high-precision HFSE systematics in TTGs," *Geochimica et Cosmochimica Acta*, vol. 75, no. 15, pp. 4157–4178, 2011.

[24] J. Adam, T. Rushmer, J. O'Neil, and D. Francis, "Hadean greenstones from the Nuvvuagittuq fold belt and the origin of the Earth's early continental crust," *Geology*, vol. 40, no. 4, pp. 363–366, 2012.

[25] J. E. Hoffmann, T. J. Nagel, C. Münker, T. Næraa, and M. T. Rosing, "Constraining the process of Eoarchean TTG formation in the Itsaq gneiss complex, southern West Greenland," *Earth and Planetary Science Letters*, vol. 388, pp. 374–386, 2014.

[26] T. J. Nagel, J. E. Hoffmann, and C. Münker, "Generation of Eoarchean tonalite-trondhjemite-granodiorite series from thickened mafic arc crust," *Geology*, vol. 40, no. 4, pp. 375–378, 2012.

[27] K. C. Condie, "TTGs and adakites: are they both slab melts?," *Lithos*, vol. 80, no. 1-4, pp. 33–44, 2005.

[28] J. Halla, "The TTG-amphibolite terrains of Arctic Fennoscandia: infinite networks of amphibolite metatexite-diatexite transitions," *Frontiers in Earth Science*, vol. 8, 2020.

[29] R. H. Smithies, D. C. Champion, and M. J. Van Kranendonk, "Formation of Paleoarchean continental crust through infracrustal melting of enriched basalt," *Earth and Planetary Science Letters*, vol. 281, no. 3-4, pp. 298–306, 2009.

[30] M. Willbold, E. Hegner, A. Stracke, and A. Rocholl, "Continental geochemical signatures in dacites from Iceland and implications for models of early Archaean crust formation," *Earth and Planetary Science Letters*, vol. 279, no. 1-2, pp. 44–52, 2009.

[31] J. H. Bédard, "A catalytic delamination-driven model for coupled genesis of Archaean crust and sub-continental lithospheric mantle," *Geochimica et Cosmochimica Acta*, vol. 70, no. 5, pp. 1188–1214, 2006.

[32] J. H. Bédard, "How many arcs can dance on the head of a plume?: A 'Comment' on: A critical assessment of Neoarchean 'plume only' geodynamics: Evidence from the Superior province, by Derek Wyman, Precambrian Research, 2012," *Precambrian Research*, vol. 229, pp. 189–197, 2013.

[33] T. E. Johnson, M. Brown, N. J. Gardiner, C. L. Kirkland, and R. H. Smithies, "Earth's first stable continents did not form by subduction," *Nature*, vol. 543, no. 7644, pp. 239–242, 2017.

[34] C. Zhang, F. Holtz, J. Koepke, P. E. Wolff, C. Ma, and J. H. Bédard, "Constraints from experimental melting of amphibolite on the depth of formation of garnet-rich restites, and

implications for models of early Archean crustal growth," *Precambrian Research*, vol. 231, pp. 206–217, 2013.

[35] O. Laurent, J. Björnsen, J.-F. Wotzlaw et al., "Earth's earliest granitoids are crystal-rich magma reservoirs tapped by silicic eruptions," *Nature Geoscience*, vol. 13, no. 2, pp. 163–169, 2020.

[36] P. Liou and J. Guo, "Generation of Archaean TTG gneisses through amphibole-dominated fractionation," *Earth*, vol. 124, no. 4, pp. 3605–3619, 2019.

[37] R. H. Smithies, Y. Lu, T. E. Johnson et al., "No evidence for high-pressure melting of Earth's crust in the Archean," *Communications*, vol. 10, no. 1, pp. 1–12, 2019.

[38] M. Jayananda, M. Guitreau, T. Tarun Thomas et al., "Geochronology and geochemistry of Meso- to Neoarchean magmatic epidote-bearing potassic granites, western Dharwar Craton (Bellur–Nagamangala–Pandavpura corridor), southern India: implications for the successive stages of crustal reworking and cratonization," *Geological Society, London, Special Publications*, vol. 489, no. 1, pp. 79–114, 2020.

[39] P. J. Sylvester, "Chapter 7 Archean granite plutons," in *Developments in Precambrian geology*, vol. 11, pp. 261–314, Elsevier, 1994.

[40] K. B. Joshi, N. Sorcar, N. C. Pant, V. Nandakumar, T. Ahmad, and J. K. Tomson, "Characterization of multiple episodes of melt generation from lower crust during Archaean using amphibole composition," *Episodes Journal of International Geoscience*, vol. 44, no. 4, pp. 443–466, 2021.

[41] G. Kumar, S. Kumar, and M. R. Mohan, "Redox series assessment, petrogenetic, and geodynamic appraisal of Neoarchean granites from the Bundelkhand craton, Central India: constraints from phase petrology and bulk rock geochemistry," *Geological Journal*, vol. 56, no. 6, pp. 3035–3063, 2021.

[42] S. Sensarma, A. Matin, D. Paul, A. Patra, A. K. Madhesiya, and G. Sarkar, "Reddening of ~2.5 Ga granitoid by high-temperature fluid linked to mafic dyke swarm in the Bundelkhand craton, north central India," *Geological Journal*, vol. 53, no. 4, pp. 1338–1353, 2018.

[43] P. K. Singh, S. K. Verma, V. K. Singh et al., "Geochronology and petrogenesis of the TTG gneisses and granitoids from the central Bundelkhand granite-greenstone terrane, Bundelkhand craton, India: implications for Archean crustal evolution and cratonization," *Precambrian Research*, vol. 359, article 106210, 2021.

[44] P. K. Singh, S. K. Verma, V. K. Singh, J. A. Moreno, E. P. Oliveira, and P. Mehta, "Geochemistry and petrogenesis of sanukitoids and high-K anatectic granites from the Bundelkhand craton, India: implications for late-Archean crustal evolution," *Journal of Asian Earth Sciences*, vol. 174, pp. 263–282, 2019.

[45] A. K. Basu, *Geology of Bundelkhand granite massif, Central India*, Records Geological Survey of India, 1986.

[46] A. Manglik, L. Adilakshmi, M. Suresh, and S. Thiagarajan, "Thick sedimentary sequence around Bahraich in the northern part of the central Ganga foreland basin," *Tectonophysics*, vol. 653, pp. 33–40, 2015.

[47] M. Ramakrishnan and R. Vaidyanadhan, *Geology of India (vol. 1 & 2)*, GSI Publications, 2010.

[48] V. K. Singh and A. Slabunov, "The central Bundelkhand Archaean greenstone complex, Bundelkhand craton, Central India: geology, composition, and geochronology of supracrustal rocks," *International Geology Review*, vol. 57, no. 11-12, pp. 1349–1364, 2015.

[49] V. K. Singh and A. Slabunov, "Two types of Archaean supracrustal belts in the Bundelkhand craton, India: geology, geochemistry, age and implication for craton crustal evolution," *Journal of the Geological Society of India*, vol. 88, no. 5, pp. 539–548, 2016.

[50] P. K. Singh, S. K. Verma, J. A. Moreno et al., "Geochemistry and Sm–Nd isotope systematics of mafic-ultramafic rocks from the Babina and Mauranipur greenstone belts, Bundelkhand craton, India: implications for tectonic setting and Paleoarchean mantle evolution," *Lithos*, vol. 330-331, pp. 90–107, 2019.

[51] A. Slabunov, V. K. Singh, K. B. Joshi, and X. Li, "Paleoarchean zircons from quartzite of south Bundelkhand supracrustal complex: origin and implications for crustal evolution in Bundelkhand craton, Central India," *Current Science*, vol. 112, no. 4, p. 794, 2017.

[52] C. L. Colleps, N. R. McKenzie, M. Sharma et al., "Zircon and apatite U-Pb age constraints from the Bundelkhand craton and Proterozoic strata of Central India: insights into craton stabilization and subsequent basin evolution," *Precambrian Research*, vol. 362, article 106286, 2021.

[53] K. B. Joshi and A. Slabunov, "Neoarchean sanukitoids from the Karelian and Bundelkhand cratons: comparison of composition, regional distribution and geodynamic setting: transactions of KarRC," *RAS*, vol. 2, pp. 1–21, 2019.

[54] P. Kaur, A. Zeh, and N. Chaudhri, "Characterisation and U-Pb-Hf isotope record of the 3.55 Ga felsic crust from the Bundelkhand Craton, northern India," *Precambrian Research*, vol. 255, pp. 236–244, 2014.

[55] P. Kaur, A. Zeh, N. Chaudhri, and N. Eliyas, "Unravelling the record of Archaean crustal evolution of the Bundelkhand craton, northern India using U-Pb zircon-monazite ages, Lu-Hf isotope systematics, and whole-rock geochemistry of granitoids," *Precambrian Research*, vol. 281, pp. 384–413, 2016.

[56] M. E. A. Mondal, J. N. Goswami, M. P. Deomurari, and K. K. Sharma, "Ion microprobe $^{207}Pb/^{206}Pb$ ages of zircons from the Bundelkhand massif, northern India: implications for crustal evolution of the Bundelkhand-Aravalli protocontinent," *Precambrian Research*, vol. 117, no. 1-2, pp. 85–100, 2002.

[57] P. Nasipuri, L. Saha, X. Hangqiang et al., *Paleoarchean Crustal Evolution of the Bundelkhand Craton, north central India*, Elsevier B.V, 2019.

[58] L. Saha, D. Frei, A. Gerdes et al., "Crustal geodynamics from the Archaean Bundelkhand craton, India: constraints from zircon U-Pb-Hf isotope studies," *Geological Magazine*, vol. 153, no. 1, pp. 179–192, 2016.

[59] L. Saha, N. C. Pant, J. K. Pati et al., "Neoarchean high-pressure margarite-phengitic muscovite-chlorite corona mantled corundum in quartz-free high-Mg, Al phlogopite-chlorite schists from the Bundelkhand craton, north central India," *Contributions to Mineralogy and Petrology*, vol. 161, no. 4, pp. 511–530, 2011.

[60] V. P. Malviya, M. Arima, J. K. Pati, and Y. Kaneko, "Petrology and geochemistry of metamorphosed basaltic pillow lava and basaltic komatiite in the Mauranipur area: subduction related volcanism in the Archean Bundelkhand craton, Central India," *Journal of Mineralogical and Petrological Sciences*, vol. 101, no. 4, pp. 199–217, 2006.

[61] A. Sahu, N. Vishwakarma, Y. Singh, and C. B. Verma, "Mineral chemistry of high-Al chromian spinel from ultramafic

rocks of the Babina–Prithvipur transect, Bundelkhand Craton, central India: implication for petrogenesis and tectonic setting," *Journal of Earth System Science*, vol. 129, no. 1, pp. 1–19, 2020.

[62] I. I. Slabunov and V. K. Singh, "Meso–Neoarchaean crustal evolution of the Bundelkhand craton, Indian shield: new data from greenstone belts," *International Geology Review*, vol. 61, pp. 1409–1428, 2019.

[63] M. E. A. Mondal and T. Ahmad, "Bundelkhand mafic dykes, central Indian shield: implications for the role of sediment subduction in Proterozoic crustal evolution," *Island Arc*, vol. 10, pp. 51–67, 2001.

[64] J. K. Pati, S. C. Patel, K. L. Pruseth et al., "Geology and geochemistry of giant quartz veins from the Bundelkhand craton, Central India and their implications," *Journal of Earth System Science*, vol. 116, no. 6, pp. 497–510, 2007.

[65] T. Radhakrishna, J. K. Tomson, R. Chandra, and C. Ramakrishna, "Geochemistry of NW-SE trending Palaeoproterozoic mafic dyke intrusions in the Bundelkhand Craton, India and subcontinental lithospheric mantle processes," *Precambrian Research*, vol. 351, article 105956, 2020.

[66] A. I. Slabunov and V. K. Singh, "Giant quartz veins of the Bundelkhand craton, Indian shield: new geological data and U-Th-Pb age," *Minerals*, vol. 12, no. 2, p. 168, 2022.

[67] A. R. Crawford, "The Precambrian geochronology of Rajasthan and Bundelkhand, northern India," *Canadian Journal of Earth Sciences*, vol. 7, no. 1, pp. 91–110, 1970.

[68] G. Kumar, S. Kumar, and K. Yi, "Three distinct Archean crustal growth events as recorded from 3.48 Ga migmatite, 2.70 Ga leucogranite, and 2.54 Ga alkali granite in the Bundelkhand craton, Central India," *Journal of Asian Earth Sciences*, vol. 219, article 104886, 2021.

[69] A. Sarkar, "Geochronology and geochemistry of mid Archaean Trondhjemitic gneisses from Bundelkhand craton, Central India," *Recent Research in Geology*, vol. 16, pp. 76–92, 1996.

[70] S. K. Verma, S. P. Verma, E. P. Oliveira, V. K. Singh, and J. A. Moreno, "LA-SF-ICP-MS zircon U-Pb geochronology of granitic rocks from the central Bundelkhand greenstone complex, Bundelkhand craton, India," *Journal of Asian Earth Sciences*, vol. 118, pp. 125–137, 2016.

[71] S. K. Singh, S. K. Rai, and S. Krishnaswami, "Sr and Nd isotopes in river sediments from the Ganga Basin: sediment provenance and spatial variability in physical erosion," *Journal of Geophysical Research: Earth Surface*, vol. 113, no. F3, p. 113, 2008.

[72] D. C. Champion and K. F. Cassidy, "Geodynamics: using geochemistry and isotopic signatures of granites to aid mineral systems studies: an example from the Yilgarn craton," *Geoscience Australia Record*, vol. 9, pp. 7–16, 2008.

[73] F. Debon and P. Le Fort, "A chemical–mineralogical classification of common plutonic rocks and associations," *Earth and Environmental Science Transactions of the Royal Society of Edinburgh*, vol. 73, no. 3, pp. 135–149, 1983.

[74] J. D. A. C. Almeida, R. Dall'Agnol, S. B. Dias, and F. J. Althoff, "Origin of the Archean leucogranodiorite-granite suites: evidence from the Rio Maria terrane and implications for granite magmatism in the Archean," *Lithos*, vol. 120, no. 3-4, pp. 235–257, 2010.

[75] M. Jayananda, D. Chardon, J. J. Peucat, and R. Capdevila, "2.61 Ga potassic granites and crustal reworking in the western Dharwar craton, southern India: tectonic, geochronologic and geochemical constraints," *Precambrian Research*, vol. 150, no. 1-2, pp. 1–26, 2006.

[76] B. C. Prabhakar, M. Jayananda, M. Shareef, and T. Kano, "Petrology and geochemistry of late archaean granitoids in the northern part of eastern Dharwar craton, southern India: implications for transitional geodynamic setting," *Journal of the Geological Society of India*, vol. 74, no. 3, pp. 299–317, 2009.

[77] I. Ahmad, M. E. A. Mondal, R. Bhutani, and M. Satyanarayanan, "Geochemical evolution of the Mangalwar complex, Aravalli craton, NW India: insights from elemental and Nd-isotope geochemistry of the basement gneisses," *Geoscience Frontiers*, vol. 9, no. 3, pp. 931–942, 2018.

[78] S. Dey, "Evolution of Archaean crust in the Dharwar craton: the Nd isotope record," *Precambrian Research*, vol. 227, pp. 227–246, 2013.

[79] S. Dey, U. K. Pandey, A. K. Rai, and A. Chaki, "Geochemical and Nd isotope constraints on petrogenesis of granitoids from NW part of the eastern Dharwar craton: possible implications for late Archaean crustal accretion," *Journal of Asian Earth Sciences*, vol. 45, pp. 40–56, 2012.

[80] M. Jayananda, D. Chardon, J. J. Peucat, Tushipokla, and C. M. Fanning, "Paleo- to Mesoarchean TTG accretion and continental growth in the western Dharwar craton, southern India: constraints from SHRIMP U-Pb zircon geochronology, whole-rock geochemistry and Nd-Sr isotopes," *Precambrian Research*, vol. 268, pp. 295–322, 2015.

[81] M. Jayananda, M. Santosh, and K. R. Aadhiseshan, "Formation of Archean (3600-2500 Ma) continental crust in the Dharwar Craton, southern India," *Earth-Science Reviews*, vol. 181, pp. 12–42, 2018.

[82] J. J. Peucat, B. Mahabaleswar, and M. Jayananda, "Age of younger tonalitic magmatism and granulitic metamorphism in the South Indian transition zone (Krishnagiri area); comparison with older Peninsular gneisses from the Gorur–Hassan area," *Journal of Metamorphic Geology*, vol. 11, no. 6, pp. 879–888, 1993.

[83] M. S. Rahaman, M. E. A. Mondal, I. Ahmad, R. Bhutani, and A. K. Choudhary, "Geochemical and Nd isotopic studies of the Neoarchaean-Palaeoproterozoic granitoids of the Aravalli craton, NW India: evidence for heterogeneous crustal evolution processes," in *Geological evolution of the Precambrian Indian Shield*, Springer, 2019.

[84] S. Sebastian, R. Bhutani, S. Balakrishnan, J. K. Tomson, and A. D. Shukla, "Geochemical and isotopic studies of potassic granite from the western Dharwar craton, southern India: implications for crustal reworking in the Neoarchean," *Geological Journal*, vol. 56, no. 6, pp. 2930–2949, 2021.

[85] J. Halla, J. van Hunen, E. Heilimo, and P. Hölttä, "Geochemical and numerical constraints on Neoarchean plate tectonics," *Precambrian Research*, vol. 174, no. 1-2, pp. 155–162, 2009.

[86] J. F. Moyen, "The composite Archaean grey gneisses: petrological significance, and evidence for a non-unique tectonic setting for Archaean crustal growth," *Lithos*, vol. 123, no. 1-4, pp. 21–36, 2011.

[87] H. Martin, J. F. Moyen, and R. Rapp, "The sanukitoid series: magmatism at the Archaean-Proterozoic transition," *Earth and Environmental Science Transactions of the Royal Society of Edinburgh*, vol. 100, pp. 15–33, 2009.

[88] Q. Qian and J. Hermann, "Formation of high-Mg diorites through assimilation of peridotite by monzodiorite magma at crustal depths," *Journal of Petrology*, vol. 51, no. 7, pp. 1381–1416, 2010.

[89] R. A. Stern and G. N. Hanson, "Archean high-Mg granodiorite: a derivative of light rare earth element-enriched monzodiorite of mantle origin," *Journal of Petrology*, vol. 32, no. 1, pp. 201–238, 1991.

[90] J. Halla, "Late Archean high-Mg granitoids (sanukitoids) in the southern Karelian domain, eastern Finland: Pb and Nd isotopic constraints on crust–mantle interactions," *Lithos*, vol. 79, no. 1-2, pp. 161–178, 2005.

[91] O. Laurent, H. Martin, R. Doucelance, J. F. Moyen, and J. L. Paquette, "Geochemistry and petrogenesis of high-K "sanukitoids" from the Bulai pluton, Central Limpopo Belt, South Africa: implications for geodynamic changes at the Archaean-Proterozoic boundary," *Lithos*, vol. 123, no. 1-4, pp. 73–91, 2011.

[92] M. A. de Oliveira, R. Dall'Agnol, and J. D. A. C. de Almeida, "Petrology of the Mesoarchean Rio Maria suite and the discrimination of sanukitoid series," *Lithos*, vol. 127, no. 1-2, pp. 192–209, 2011.

[93] M. A. de Oliveira, R. Dall'agnol, and B. Scaillet, "Petrological constraints on crystallization conditions of Mesoarchean sanukitoid rocks, southeastern Amazonian craton, Brazil," *Journal of Petrology*, vol. 51, no. 10, pp. 2121–2148, 2010.

[94] J. Semprich, J. A. Moreno, and E. P. Oliveira, "Phase equilibria and trace element modeling of Archean sanukitoid melts," *Precambrian Research*, vol. 269, pp. 122–138, 2015.

[95] J. Halla, "Pb isotopes - a multi-function tool for assessing tectonothermal events and crust-mantle recycling at late Archaean convergent margins," *Lithos*, vol. 320-321, pp. 207–221, 2018.

[96] W. Bleeker, "The late Archean record: a puzzle in ca. 35 pieces," *Lithos*, vol. 71, no. 2-4, pp. 99–134, 2003.

[97] R. H. Smithies and D. C. Champion, "The Archaean high-mg diorite suite: links to tonalite–trondhjemite–granodiorite magmatism and implications for early Archaean crustal growth," *Journal of Petrology*, vol. 41, no. 12, pp. 1653–1671, 2000.

[98] J. Fu, S. Liu, B. Zhang, R. Guo, and M. Wang, "A Neoarchean K-rich granitoid belt in the northern North China craton," *Precambrian Research*, vol. 328, pp. 193–216, 2019.

[99] G. Sun, S. Liu, M. Wang, H. Bao, and G. Teng, "Complex Neoarchean mantle metasomatism: evidence from sanukitoid diorites-monzodiorites-granodiorites in the northeastern North China craton," *Precambrian Research*, vol. 342, article 105692, 2020.

[100] B. P. Radhakrishna, "Suspect tectono-stratigraphic terrane elements in the Indian subcontinent," *ournal of Geological Society of India (Online archive from Vol 1 to Vol 78)*, vol. 34, pp. 1–24, 1989.

[101] M. E. A. Mondal, K. K. Sharma, A. Rahman, and J. N. Goswami, "Ion microprobe $^{207}Pb/^{207}Pb$ zircon ages for gneiss-granitoid rocks from Bundelkhand massif: Evidence for Archaean components," *Current Science*, vol. 74, pp. 70–75, 1998.

[102] S. Kumar, K. Yi, K. Raju, M. Pathak, N. Kim, and T. H. Lee, "SHRIMP U-Pb geochronology of felsic magmatic lithounits in the central part of Bundelkhand Craton, Central India," in *7th Hutton symposium on granites and related rocks*, vol. 83, Avila, Spain, 2011.

[103] V. R. Pradhan, J. G. Meert, M. K. Pandit, G. Kamenov, and M. E. A. Mondal, "Paleomagnetic and geochronological studies of the mafic dyke swarms of Bundelkhand craton, central India: Implications for the tectonic evolution and paleogeographic reconstructions," *Precambrian Research*, vol. 198, pp. 51–76, 2012.

[104] M. Jayananda, K. R. Aadhiseshan, M. A. Kusiak et al., "Multistage crustal growth and Neoarchean geodynamics in the eastern Dharwar craton, southern India," *Gondwana Research*, vol. 78, pp. 228–260, 2020.

[105] M. Jayananda, H. Martin, J.-J. Peucat, and B. Mahabaleswar, "Late Archaean crust-mantle interactions: geochemistry of LREE-enriched mantle derived magmas. Example of the Closepet batholith, southern India," *Contributions to Mineralogy and Petrology*, vol. 119, no. 2-3, pp. 314–329, 1995.

[106] M. Guitreau, J. Blichert-Toft, H. Martin, S. J. Mojzsis, and F. Albarède, "Hafnium isotope evidence from Archean granitic rocks for deep-mantle origin of continental crust," *Earth and Planetary Science Letters*, vol. 337-338, pp. 211–223, 2012.

[107] M. R. Mohan, S. J. Piercey, B. S. Kamber, and D. S. Sarma, "Subduction related tectonic evolution of the Neoarchean eastern Dharwar craton, southern India: new geochemical and isotopic constraints," *Precambrian Research*, vol. 227, pp. 204–226, 2013.

[108] M. R. Mohan, D. S. Sarma, N. J. McNaughton et al., "SHRIMP zircon and titanite U-Pb ages, Lu-Hf isotope signatures and geochemical constraints for ~2.56 Ga granitic magmatism in Western Dharwar craton, southern India: evidence for short-lived Neoarchean episodic crustal growth?," *Precambrian Research*, vol. 243, pp. 197–220, 2014.

[109] M. Santosh, Q.-Y. Yang, E. Shaji, M. R. Mohan, T. Tsunogae, and M. Satyanarayanan, "Oldest rocks from peninsular India: evidence for Hadean to Neoarchean crustal evolution," *Gondwana Research*, vol. 29, no. 1, pp. 105–135, 2016.

[110] M. Santosh, Q. Y. Yang, E. Shaji, T. Tsunogae, M. R. Mohan, and M. Satyanarayanan, "An exotic Mesoarchean microcontinent: the Coorg Block, southern India," *Gondwana Research*, vol. 27, pp. 165–195, 2015.

[111] C. Wang, S. Song, Y. Niu, C. Wei, and L. Su, "TTG and potassic granitoids in the eastern North China craton: making Neoarchean upper continental crust during microcontinental collision and post-collisional extension," *Journal of Petrology*, vol. 57, no. 9, pp. 1775–1810, 2016.

[112] G. Zhao and P. A. Cawood, "Precambrian geology of China," *Precambrian Research*, vol. 222-223, pp. 13–54, 2012.